

---

# ON THE PRIVACY OF LLMs: AN ABLATION STUDY

---

**Karima Makhoulouf**  
UDST, Doha, Qatar  
karima.makhoulouf@udst.edu.qa

**Lamiaa Basyoni**  
UDST, Doha, Qatar  
Lamiaa.Basyoni@udst.edu.qa

**Syed Khaderi**  
UDST, Doha, Qatar  
60317695@udst.edu.qa

**Gabriel Marquez**  
UDST, Doha, Qatar  
60300343@udst.edu.qa

**Peter Sotomango**  
UDST, Doha, Qatar  
60301211@udst.edu.qa

**Mahmoud Awawdah**  
UDST, Doha, Qatar  
60307557@udst.edu.qa

**Sami Zhioua**  
UDST, Doha, Qatar  
sami.zhioua@udst.edu.qa

## ABSTRACT

Large language models (LLMs) are increasingly deployed in interactive and retrieval-augmented settings, raising significant privacy concerns. While attacks such as Membership Inference (MIA), Attribute Inference (AIA), Data Extraction (DEA), and Backdoor Attacks (BA) have been studied, they are typically analyzed in isolation, leaving a gap in understanding their behavior under common system factors. In this paper, we introduce a unified threat model and notation, reproduce a representative set of privacy attacks, and conduct a structured ablation study to evaluate the impact of key factors such as model architecture, scale, dataset characteristics, and retrieval configuration. Our analysis reveals clear differences across attack types. Membership inference attacks, particularly mask-based variants, exhibit strong and reliable signals, while backdoor attacks achieve consistently high success rates due to their trigger-based nature. In contrast, attribute inference and data extraction attacks remain more challenging, resulting in lower accuracy, yet they pose significant risks as they target sensitive personal information. Overall, these results highlight that privacy risks in LLM systems are highly context-dependent and driven by design choices, emphasizing the need for holistic evaluation and informed deployment practices.

**Keywords** Large Language Models · Privacy · Privacy Attacks · Membership Inference Attacks · Data Extraction Attacks · LLM · MIA

## 1 Introduction

Large Language Models (LLMs) have rapidly evolved from static predictive models to highly interactive systems that continuously process user prompts, conversational context, and externally retrieved information. Deployed at scale across domains such as healthcare, education, customer support, and software development, LLMs increasingly operate as socio-technical systems whose behavior emerges from complex interactions between training data, model architecture, system prompts, and user input [1]. While these capabilities enable powerful applications, they also raise significant concerns regarding user privacy.

Early work on privacy in machine learning primarily focused on memorization and overfitting, leading to the development of formal privacy attacks such as Data Extraction Attacks (DEAs) [2, 3] and Membership Inference Attacks (MIAs) [4, 5]. These works established that models which generalize well may nonetheless leak information about individual training records. In the context of LLMs, this line of research has expanded substantially, demonstrating that large models may unintentionally memorize rare or sensitive training samples, expose membership information, or retain vulnerabilities introduced during fine-tuning or alignment. These studies also demonstrated that memorization scales with model capacity, training duration, and data duplication, making LLMs particularly vulnerable to training data exposure [6, 7].

In parallel, a growing body of work has revealed that LLMs can leak sensitive information such as age, location, or occupation even in the absence of explicit adversarial intent, by inferring personal attributes from free-form text, conversational cues, or interaction history [8]. We refer to this type of privacy risk as Attribute Inference Attacks (AIAs). Backdoor Attacks (BAs), on the other hand, embed hidden triggers that induce targeted malicious behaviors at inference time [9].

Despite rapid progress, existing research on LLM privacy remains fragmented. Privacy attacks, including AIAs, DEAs, MIAs, and BAs, are typically studied in isolation, each under different threat models, assumptions, and evaluation metrics. This fragmentation makes it difficult for researchers and practitioners to reason holistically about privacy risks in real-world LLM deployments. As a result, it remains unclear how these seemingly distinct privacy risks relate to one another, whether they share common underlying drivers, and how design choices across the LLM lifecycle jointly influence these privacy risks.

In this work, we argue that the aforementioned attacks—representative of the main privacy attacks proposed in the literature—should be understood within a single, unified threat landscape spanning the entire LLM lifecycle from data collection and pretraining to fine-tuning, deployment, and inference-time interaction. To this end, we introduce a common threat model, notation, and taxonomy that captures these privacy attacks within a common framework. Additionally, we perform a systematic empirical

ablation study to quantify how key factors such as model scale, training data properties and scale, and inference-time parameters affect the success of these privacy attacks.

Our contributions are summarized as follows:

- We propose a unified threat model and notation that connects AIAs, DEAs, MIAs, and BAs within a common privacy landscape, enabling consistent reasoning across different attack objectives.
- We reproduce a representative set of privacy attacks on LLMs within a shared experimental framework, contributing to a systematization of knowledge and improving the reproducibility and comparability of prior work.
- We conduct a structured empirical ablation study to evaluate how architectural, training, and inference-time factors jointly influence these attacks, identifying both shared trends and attack-specific sensitivities.
- We derive actionable insights and practical recommendations, highlighting how specific design choices (e.g., model architecture, scale, dataset characteristics, and retrieval configuration) impact privacy risks, and providing guidance for the development of privacy-aware LLM systems.

Overall, we present a unified ablation framework to understand how LLM design choices impact AIAs, DEAs, MIAs, and BAs, providing a foundation for more informed and privacy-aware LLM design.

## 2 Background & Notation

LLMs introduce privacy risks that differ fundamentally from those of traditional machine learning systems due to their scale, generative nature, and continuous interaction with users. In this section, we introduce the key concepts and necessary background and notation required to analyze the four privacy risks considered in this study, namely AIAs, DEAs, MIAs, and BAs. Our goal is to provide a unified perspective that links core properties of LLMs to these attacks, enabling a systematic analysis of their underlying mechanisms and impact factors.

**LLM Lifecycle and Privacy Surfaces.** We consider the lifecycle of an LLM as a sequence of stages: (i) data collection and preprocessing, (ii) pre-training, (iii) fine-tuning and alignment, and (iv) deployment and inference.

Each stage introduces distinct privacy surfaces. Training stages (pre-training and fine-tuning) determine how information is encoded into model parameters, while the inference stage governs how this information can be exposed through model outputs.

Privacy risks manifest differently across these stages. For instance, DEAs primarily exploit memorized information

acquired during training, whereas MIAs rely on behavioral differences between training and non-training samples observable at inference time. AIAs are predominantly inference-time attacks driven by contextual reasoning. BAs are typically injected during model pretraining/ fine-tuning using poisoned data but activated during inference.

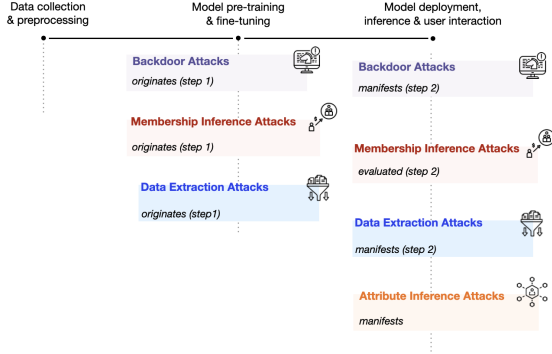


Figure 1: Mapping MIAs, DEAs, AIAs, and BAs to Privacy Surfaces Across the LLM Lifecycle

Fig. 1 provides a unified visualization of the LLM lifecycle stages and maps each privacy attack to the stages where it typically originates and/or manifests.

**Memorization vs Inference.** A fundamental distinction in privacy of LLMs is between *memorization* and *inference*. *Memorization* refers to the model’s tendency to store and reproduce specific training examples or rare sequences. In contrast, *inference* refers to the model’s ability to derive latent or sensitive attributes from input context without explicitly memorizing them.

DEA is primarily driven by *memorization*, as it aims to recover training data verbatim or near-verbatim. MIA is partially related to *memorization* through overfitting signals. In contrast, AIA is driven by *inference*, where the model predicts sensitive attributes from contextual cues. BA introduces conditional behaviors that are neither purely *memorization* nor *inference*, but rather trigger-dependent mappings learned during training.

**Access Model.** MIA and AIA are typically conducted in black-box settings, relying only on model outputs. DEA can operate in both black-box and white-box regimes, with stronger guarantees under the latter. BAs require at least grey-box access for injection, but can be exploited in black-box settings. In this study, we consider black-box access for AIA, MIA, and DEA. However, for the BA, we assume a training-time adversary with white-box access, while the attack is executed at inference time under a black-box setting.

**Granularity of Risk.** Privacy risks can occur at different levels of granularity. AIA operates at the attribute level, inferring sensitive properties (e.g., demographic or health attributes). DEA targets record-level leakage, aiming to

reconstruct specific training samples. MIA also operates at the record level by determining membership. BA can induce record-level leakage when used to trigger data extraction.

The four privacy attacks considered in this work can be interpreted as specific combinations of the above dimensions. This unified perspective provides a foundation for our ablation study, enabling systematic analysis of how different factors influence each class of privacy attacks.

Table 1 summarizes how the privacy attacks map onto the aforementioned LLM privacy risk dimensions.

### 2.1 Notations

Table 2 summarizes the notation used throughout the paper, including the symbols needed later for AIA, DEA, MIA, and BA.

**Evaluation Perspective.** Throughout this paper, privacy risks are empirically evaluated through ablation studies that analyze how changes in model architecture, training procedure, prompting strategy, or system design affect different privacy threats. Rather than treating privacy issues in isolation, our analysis emphasizes shared drivers, trade-offs, and interactions across the LLM lifecycle. In the following sections (Sections 3, 4, 5, and 6), we present the four privacy attacks considered in this study, highlighting their mechanisms, impact factors, and evaluation metrics.

## 3 Membership Inference Attack (MIA)

A Membership Inference Attack (MIA) is a privacy attack in which an adversary  $\mathcal{A}$  determines whether a candidate record belongs to a dataset  $D$ . Given a membership bit  $b \in \{0, 1\}$  ( $b=1$ : member,  $b=0$ : non-member), the adversary produces a guess  $\hat{b}$ ; the attack succeeds when  $\hat{b} = b$ .

In RAG, the system comprises an external database  $\mathcal{D} = \{d_1, d_2, \dots, d_n\}$ , a retriever  $R$ , and an LLM  $\mathcal{M}$ . Given a query  $Q$ , the retriever computes similarity  $S = \text{Sim}(Q, d_i)$  for each  $d_i \in \mathcal{D}$  and selects a context set  $D_s = R(Q, \mathcal{D}, S)$  for  $\mathcal{M}$ . Given a target sample  $x_t$ , a complete record whose membership in  $\mathcal{D}$  is unknown, the adversary’s goal is:

$$\mathcal{A}(x_t | \mathcal{D}, R, \mathcal{M}) \rightarrow \text{Member/Non-Member}, \quad (1)$$

where Member (resp. Non-Member) indicates  $x_t \in \mathcal{D}$  (resp.  $x_t \notin \mathcal{D}$ ). The attacker has only black-box query access and knowledge of  $\mathcal{D}$ ’s distribution, with no access to  $\mathcal{M}$ ’s parameters,  $R$ ’s configuration, nor any sample in  $\mathcal{D}$ .

In the following we consider two variants of MIA namely, S2MIA and MBMIA.

Table 1: Mapping of the privacy attacks across key LLM privacy risk dimensions.

LLM Dimension	Privacy Attack	DEA	MIA	AIA	BA
Lifecycle Stage (Origin)		Training + Inference	Training + Inference	Inference	Training + Inference
Lifecycle Stage (Exploitation)		Inference	Inference	Inference	Inference
Access Model		Black-box	Black-box	Black-box	White (injection), Black (trigger)
Granularity of Leakage		Record-level	Record-level	Attribute-level	N/A
Attack Objective		Data extraction	Membership inference	Attribute inference	Output manipulation

### 3.1 Semantic Similarity-based Membership Inference Attack (S2MIA)

#### 3.1.1 Mechanism

The core intuition behind S2MIA [10] is the following. If a document is stored in a RAG system’s knowledge base, then querying the system about that document’s content should produce a response that closely resembles the original document. Conversely, if the document is absent, the LLM must rely on its own parametric knowledge, producing a less faithful response. S2MIA exploits this asymmetry by measuring how closely the RAG system’s output matches a target document, using the degree of similarity as a membership signal.

Concretely, the attack proceeds in three stages. First, the target sample  $x_t$  is split into two complementary parts: a *query portion*  $x_t^q$ , which is used to prompt the RAG system, and a *held-out portion*  $x_t^r$ , which is reserved for comparison (i.e.,  $x_t = x_t^q \oplus x_t^r$ , where  $\oplus$  denotes concatenation). In QA datasets, the question naturally serves as  $x_t^q$  and the answer as  $x_t^r$ .

Second, the query  $x_t^q$  is submitted to the target RAG system. Internally, the retriever  $R$  selects the most relevant documents  $D_s$  from the external database  $\mathcal{D}$  and provides them as context to the LLM  $\mathcal{M}$ , which generates a response  $\bar{x}^g$ . If  $x_t \in \mathcal{D}$ , the retriever is likely to surface it within  $D_s$ , causing  $\bar{x}^g$  to closely reflect the content of  $x_t$ . If  $x_t \notin \mathcal{D}$ , the model generates from parametric knowledge alone, producing a less similar output.

Third, two membership features are extracted from the response. The *semantic similarity*  $S_{sem} = BLEU(x_t, \bar{x}^g)$  measures the  $n$ -gram overlap between the target sample and the generated output; member samples are expected to yield higher BLEU scores. The *generation perplexity*  $PPL_{gen}$  measures the LLM’s average uncertainty when producing  $\bar{x}^g$ ; member samples, whose content is reinforced by retrieved context, are expected to yield lower perplexity. A logistic regression classifier trained on a labeled reference dataset  $D_r$  of known members and non-members uses these two features to perform the final membership inference.

#### 3.1.2 Factors Affecting the Attack

We consider the following six factors for our ablation study. The Dataset factor  $\mathcal{D}$  (Compared to two RAG datasets used in [10], we used four RAG datasets described below.). The Corpus size factor corresponds to the number

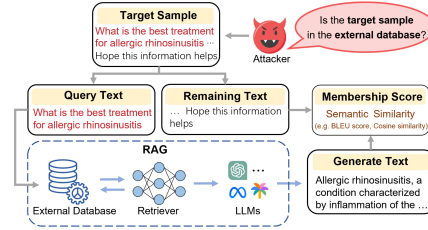


Figure 2: S2MIA Attack. (Figure from [10])

of QA pairs. We considered portions of the full corpus of each dataset ranging from 10% to 100%. The LLM model ( $\mathcal{M}$ ) factor. We considered five LLM models different from the models in [10], except for the baseline model (Llama-2-7b-chat-hf). The membership ratio factor which corresponds to the ratio of member samples (belonging to the RAG dataset) in the set of samples used in each attack testing experiment. We used ratios ranging from 60% to 90%. The embedding model factor. We used four different embedding models. And finally the prompt style factor, which refers to the structural template used to format the query  $x_t^q$  before submitting it to the RAG system. Different prompt styles guide the LLM to produce responses with varying levels of structure, reasoning, and verbosity, which in turn affects the BLEU and perplexity signals exploited by the attack. We considered four prompt styles: the Regular style (baseline) used in [10], which submits the query directly, RTOC (Role-Task-Output-Context), Chain of Thought (CoT), which prompts step-by-step reasoning, and CRISPE (Capacity-Role-Insight-Statement-Personality-Experiment).

#### 3.1.3 Metrics

$F1$  score proved unreliable due to *recall inflation*: under weak signals the classifier tends to predict “member” for nearly all inputs. Therefore, similarly to Li et al. [10], we used ROC AUC and PR AUC as primary metrics.

#### 3.1.4 Experimental Results and Analysis

In the following, we present the experimental evaluation of S2MIA under a controlled ablation framework. Each experiment isolates a specific factor while keeping all other components fixed at baseline settings.

We use the following four datasets to test this MIA attack:

Table 2: Notation used throughout the paper.

Symbol	Meaning
$M$	Target LLM.
$f_\theta$	Parametric model with parameters $\theta$ .
$D$	Dataset (pre-training, fine-tuning, or observed user-text dataset depending on context).
$S$	System prompt (hidden in some threat models) or a set of training samples (context-dependent).
$P$	User-facing prompt content.
$u$	User identity index in a dataset of users.
$t$	Text authored by user $u$ (free text, posts, messages).
$\mathcal{A}$	Adversary.
$pre, suf$	Prefix, Suffix.
<b>AIA-specific notation</b>	
$\mathcal{A}_1, \mathcal{A}_2$	Adversaries in (respectively) passive free-text inference and active adversarial interaction settings.
$P_{\mathcal{A}_1}(t) = (S, P)$	Prompt construction from text $t$ for contextual inference.
$F_{\mathcal{A}_1}(t)$	Fixed wrapper strings and formatting function embedding $t$ .
$\{(a_j, v_j)\}_{j=1}^k$	$k$ inferred attribute–value tuples output by $M$ .
$a, u_a$	Sensitive attribute $a$ and ground-truth value $u_a$ (when available) for user $u$ .
$T_p, T_h$	Public task, hidden malicious task embedded in a system prompt (adversarial interaction).
$m_i, r_i^p, r_i^h$	User message $m_i$ , public response $r_i^p$ , hidden/internal response $r_i^h$ at round $i$ .
<b>DEA-specific notation</b>	
$z = [pre \parallel suf]$	Training instance decomposed into known prefix $pre$ and target suffix $suf$ to be recovered by extraction.
$s[r]$	Canary template instantiated with randomness $r$ (synthetic secret).
$rank_\theta(s[r])$	Rank of secret among all candidates sorted by log-perplexity.
$exposure_\theta(s[r])$	Exposure metric quantifying memorization of $s[r]$ .
$v$	A specific PII value (e.g., an email address or phone number string).
$\tau$	PII type label (e.g., EMAIL, PHONE, STRUCTURED_NAME).
$R$	Candidate pool of size $N$ ; contains the true secret $v$ and $N-1$ random alternatives.
$N =  R $	Candidate pool size ( $N = 501$ in this work).
$P_{z, \theta}(\cdot)$	Average negative log-probability (log-perplexity) of a sequence under $f_\theta^M$ ; see Eq. (5).
$\hat{s}_{1:k}$	Partial token sequence of length $k$ during Dijkstra search.
$w(\cdot \rightarrow \cdot)$	Non-negative edge weight in the Dijkstra token graph; see Eq. (8).
$\mathcal{V}$	Model vocabulary; $ \mathcal{V}  = 50,257$ for GPT-Neo.
$K$	Number of top tokens expanded at each Dijkstra node.
<b>MIA-specific notation</b>	
$C$	Challenger in the membership-inference security game.
$b \in \{0, 1\}$	Membership bit (1: member sample drawn from $D$ ; 0: non-member).
$(x, y)$	Candidate data record (input, label).
$\hat{b} \in \{0, 1\}$	Adversary’s membership guess (security game output).
$Q_{in}(x, y), Q_{out}(x, y)$	Distributions over trained models with/without $(x, y)$ included.
$\tilde{Q}_{in}(x, y), \tilde{Q}_{out}(x, y)$	Model’s loss distributions with/without $(x, y)$ included.
$\Lambda(f; x, y)$	Likelihood ratio used for hypothesis testing view of membership inference.
$\ell(f(x), y)$	Loss statistic often used as a tractable proxy for membership tests.
<b>MBA-specific notation (RAG framework)</b>	
$\mathcal{D}$	Knowledge database comprising a collection of documents.
$d$	Target document whose membership in $\mathcal{D}$ is being inferred.
$k$	Number of relevant documents retrieved from the database.
$\mathcal{P}_k$	Retrieved documents, calculated as $\text{RETRIEVE}(q, \mathcal{D}, k)$ .
$s$	System prompt used to guide the LLM’s generation.
$r$	Generated response, calculated as $\text{LLM}(s \oplus Q_d \oplus \mathcal{P}_k)$ .
$Q_d$	Document-specific question generated from $d$ (masked target document).
$\text{BMIC}(d, r)$	Binary Membership Inference Classifier predicting probability $P(d \in \mathcal{D})$ .
$M$	Hyperparameter defining the number of masked words or phrases in $d$ .
$\gamma$	Hyperparameter defining the threshold fraction for mask prediction accuracy ( $\gamma \in (0, 1]$ ).
$\oplus$	Concatenation operation.
<b>BA-specific notation</b>	
$\theta, \theta'$	Clean vs. compromised parameters (e.g., after backdoor injection).
$x, x'$	Clean input vs. triggered input (activates the backdoor).
$\tau(\cdot)$	Trigger transformation applied to a clean input $x$ to obtain $x' = \tau(x)$ .

Table 3: Attack performance across datasets.

Dataset	Accuracy	Precision	ROC AUC	PR AUC
NQ-Open	0.610	0.604	0.662	0.601
TriviaQA	0.510	0.505	0.577	0.593
SQuAD	0.820	0.767	<b>0.895</b>	<b>0.896</b>
HotpotQA	0.820	0.848	0.858	0.842

- **NQ-Open** (Natural Questions Open): A large-scale open-domain question answering dataset derived from real Google search queries, where answers are short spans from Wikipedia.
- **TriviaQA**: A question answering dataset consisting of trivia questions paired with evidence documents, designed to test reading comprehension and knowledge retrieval from multiple sources.
- **SQuAD** (Stanford Question Answering Dataset): A widely used reading comprehension dataset where models answer questions based on a given passage from Wikipedia.
- **HotpotQA**: A multi-hop question answering dataset requiring reasoning across multiple documents to answer complex questions.

The baseline configuration consists of selecting a set of 2000 samples (QA sentence) from which 80% are members and 20% non-members, using Llama-2-7b-chat-hf as the LLM model ( $\mathcal{M}$ ), Contriever-msmarco as the retriever, NQ-Open as the RAG dataset, and 100% of the corpus. Across all experiments except Experiment A, the baseline dataset NQ-Open is used.

### Experiment 3.1.A — Dataset Domain Impact

The first experiment isolates the effect of the RAG dataset  $\mathcal{D}$  by repeating the baseline attack across all four datasets while keeping the LLM, retriever, corpus size, and membership ratio fixed.

Table 3 shows the dominant effect of dataset choice: SQuAD and HotpotQA achieved ROC AUC of 0.895 and 0.858, respectively, while TriviaQA (AUC = 0.577) barely exceeds random chance. PR AUC follows a similar pattern, confirming that discrimination is not an artifact of threshold selection.

### Experiment 3.1.B — Data Size Impact

The second experiment isolates the effect of corpus size by repeating the baseline attack on increasingly larger portions of the NQ-Open corpus (10%, 25%, 50%, 75%, 100%)<sup>1</sup>, while keeping the LLM, retriever, and membership ratio fixed.

As shown in Table 4, ROC AUC of the attack increased monotonically from 0.472 at 25% to 0.690 at 100% corpus size. At 10–50%, the attack degenerated to at or below random-chance performance, contradicting [10] finding that smaller corpora are easier to attack.

<sup>1</sup>The sampling of the portion is done randomly.

Table 4: Attack performance across increasingly large corpus size

Corpus Size	Accuracy	Precision	ROC AUC	PR AUC
10%	0.480	0.488	0.478	0.501
25%	0.480	0.488	0.472	0.509
50%	0.480	0.488	0.536	0.529
75%	0.620	0.620	0.594	0.564
100%	0.610	0.612	<b>0.690</b>	<b>0.616</b>

Table 5: Attack performance across membership ratios.

Member Ratio	Accuracy	Precision	ROC AUC	PR AUC
60%	0.730	0.709	<b>0.799</b>	<b>0.811</b>
70%	0.760	0.710	0.769	0.721
80%	0.600	0.593	0.656	0.579
90%	0.650	0.660	0.692	0.667

Table 6: Attack performance across LLM models

LLM Model	Accuracy	Precision	ROC AUC	PR AUC
TinyLlama-1.1B-Chat-v1.0	0.600	0.583	0.554	0.566
gemma-2b-it	0.460	0.478	0.588	0.611
Mistral-7B-Instruct-v0.2	0.600	0.574	0.561	0.554
Llama-2-7b-chat-hf	0.590	0.596	<b>0.677</b>	<b>0.602</b>
Qwen2-1.5B-Instruct	0.650	0.632	0.519	0.566

### Experiment 3.1.C — Membership Ratio Impact

The third experiment isolates the effect of the membership ratio by varying the proportion of member samples in the test set (60%, 70%, 80%, 90%), while keeping the LLM, retriever, dataset (NQ-Open), and corpus size fixed to baseline settings.

Table 5 shows that lower ratios in the tested range (60–70%) produced stronger discrimination (AUC = 0.799 and 0.769) compared to higher ratios (80–90%). A sharp drop occurred between 70% and 80%, likely due to fewer non-member training examples and retrieval of related member content, blurring the BLEU signal.

### Experiment 3.1.D — Model Architecture Impact

The fourth experiment isolates the effect of the LLM model ( $\mathcal{M}$ ) by repeating the baseline attack with five different models (different from the models used in [10]), while keeping the retriever, dataset (NQ-Open), corpus size, and membership ratio fixed.

As shown in Table 6, Llama-2-7b-chat-hf achieved the highest ROC AUC (0.677) while scores remained relatively compressed across all models, confirming the limited influence of LLM choice relative to other factors.

### Experiment 3.1.E — Embedding Model Impact

The fifth experiment isolates the effect of the embedding model used by the retriever, by repeating the baseline attack with four additional embedding models alongside the baseline Contriever-msmarco, while keeping the LLM,

Table 7: Attack performance across embedding models

Embedding Model	Accuracy	Precision	ROC AUC	PR AUC
contriever-msmarco	0.620	0.615	0.670	0.615
multi-qa-mpnet-base-dot-v1	0.620	0.620	0.658	0.593
all-MiniLM-L6-v2	0.640	0.630	<b>0.734</b>	<b>0.683</b>
all-mpnet-base-v2	0.640	0.640	0.674	0.627
bge-base-en-v1.5	0.570	0.564	0.650	0.590

Table 8: Attack performance across prompt styles.

Prompt Style	Accuracy	Precision	ROC AUC	PR AUC
Regular	0.580	0.583	0.620	0.567
RTOC	0.620	0.620	<b>0.624</b>	0.680
Chain of Thought	0.630	0.600	0.570	0.544
CRISPE	0.590	0.596	0.616	<b>0.684</b>

dataset (NQ-Open), corpus size, and membership ratio fixed.

As shown in Table 7, all-MiniLM-L6-v2 achieved the best ROC AUC (0.734), but the overall spread remained small (0.084), indicating a similarly limited influence on the LLM model factor.

### Experiment 3.1.F — Prompt Style Impact

The sixth experiment isolates the effect of the prompt style used to query the RAG system by repeating the baseline attack with four different prompting strategies: Regular (baseline), RTOC, Chain of Thought (CoT), and CRISPE, while keeping the LLM, retriever, dataset (NQ-Open), corpus size, and membership ratio fixed.

As shown in Table 8, the Regular and RTOC styles achieved the highest ROC AUC scores (0.620 and 0.624, respectively), followed closely by CRISPE (0.616), while Chain of Thought produced the lowest discrimination (ROC AUC = 0.570). Notably, CoT exhibited the highest recall (0.78) but the lowest precision (0.600), suggesting it triggers a bias toward predicting “member” rather than improving genuine discrimination. The BLEU threshold values varied substantially across styles—Regular produced the highest threshold (27.52), reflecting higher overall  $n$ -gram overlap in its responses, whereas CoT yielded the lowest (0.30), consistent with its verbose, reasoning-heavy outputs diluting lexical similarity. PR AUC further separates the styles: CRISPE (0.684) and RTOC (0.680) outperformed Regular (0.567) and CoT (0.544), suggesting that structured prompting styles may yield better-calibrated membership signals despite similar ROC AUC. Overall, prompt style had a moderate effect on attack performance, with all styles remaining in a narrow ROC AUC band (0.570–0.624).

### Summary

Figure 3 presents a grouped bar chart of ROC AUC scores across all experiment groups and conditions. The dataset group shows the strongest contrast, with SQuAD (0.895) and HotpotQA (0.858) substantially outperforming NQ-

Open (0.662) and TriviaQA (0.577). Corpus size showed a clear monotonic trend from 0.472 at 25% to 0.690 at 100%. Across LLM models and embedding models, ROC AUC scores remain relatively compressed, confirming their limited influence relative to dataset and corpus size. Prompt style showed similarly limited variation, with all four styles remaining in a narrow ROC AUC band (0.570–0.624).

Key limitations include the absence of confidence intervals from single-seed experiments, an untested balanced membership ratio (50%), inconsistent perplexity behavior across models (notably gemma-2b-it exceeding 250,000), and the fact that most configurations across the LLM and embedding axes barely exceeded random-chance performance.

## 3.2 Mask-Based Membership Inference Attack (MBMIA)

Similarly to the previous attack (S2MIA), MBMIA [11] has the same goal. That is, given a target document  $d$ , an adversary aims to determine whether  $d$  was included in the retriever ( $R$ )’s indexed corpus (“Member”) or not (“Non-Member”) of the RAG Dataset  $\mathcal{D}$ . Given a user query  $Q$  and a RAG dataset  $\mathcal{D}$ , the retriever  $R$  returns the top- $K$  documents

$$D_K = R(Q, \mathcal{D}, K), \tag{2}$$

and the generator then produces a response using the system prompt  $s$ , a document-specific probe  $Q_d$ , and the retrieved context:

$$r = \mathcal{M}(s \oplus Q_d \oplus D_K). \tag{3}$$

**Threat Model.** We assume the black-box setting used by in [11]: the attacker cannot access the index contents, retriever  $R$  internals, embedding vectors, or model  $\mathcal{M}$  weights, but can repeatedly query the deployed RAG system and observe only its textual outputs  $D_K$ . The goal is to build a binary membership inference classifier (BMIC) that outputs the likelihood of  $d \in \mathcal{D}$ :

$$P(d \in \mathcal{D}) = \text{BMIC}(d, r). \tag{4}$$

### 3.2.1 Mechanism

Our implementation keeps the core mechanism as Liu et al.[11], but our experiments differ in two important ways. First, we explicitly compare a hosted GPT model and local open-weight models. Second, we extend beyond the original three datasets and probe additional system factors such as retrieval depth and index size.

The main goal of MBMIA is to assess the efficiency of the MIA using masks. The basic idea is to mask terms in the query based on a target document  $d$  which can efficiently indicate whether  $d \in \mathcal{D}$ . More precisely, MBMIA works because it masks terms that are intentionally difficult to reconstruct from general background knowledge alone. If  $d$  itself is retrieved, the generator receives the exact lexical evidence needed to recover those terms. If the target

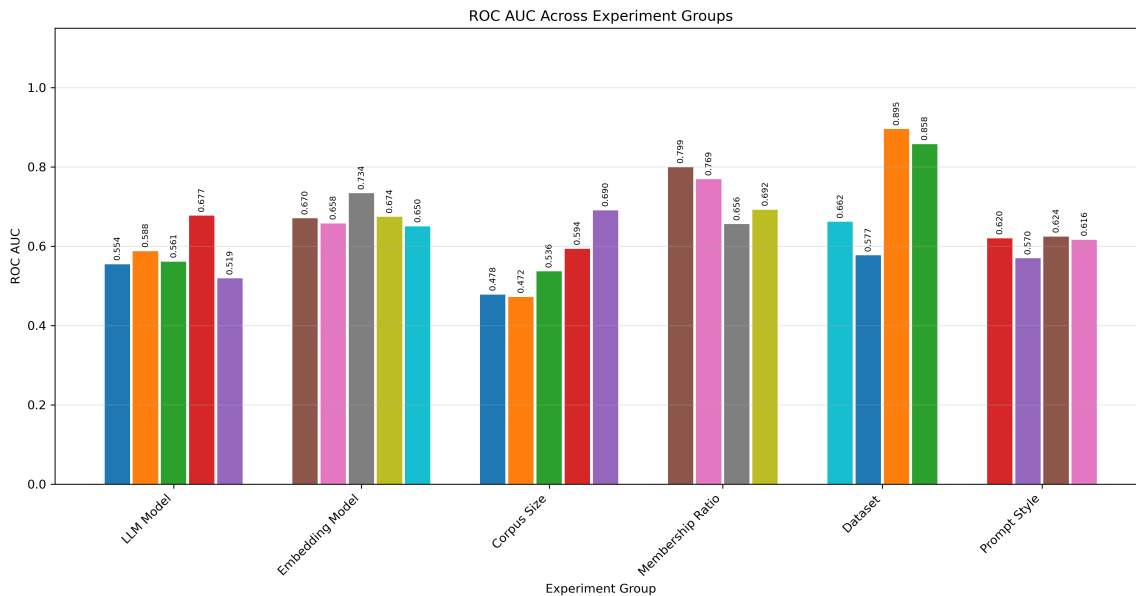


Figure 3: Grouped bar chart of ROC AUC scores across all experiment groups. The dataset group shows the strongest contrast, while LLM model, embedding model, and prompt style groups remain in narrow bands.

document is absent ( $d \notin \mathcal{D}$ ), the model may still produce plausible paraphrases, broad concepts, or approximate answers, but it should fail more often on exact reconstruction [11]. That exact-match asymmetry is what makes mask accuracy useful as a membership signal.

The end-to-end attack pipeline is as follows.

1. **Proxy scoring.** A proxy language model is used to estimate which words or phrases are hardest to predict from local context alone; the masking policy targets those difficult units rather than random words [11]. This is better described as a *difficulty ranking* step than as a generic perplexity computation.
2. **Mask generation.** The selected terms are replaced with placeholders such as [Mask\_1], while preserving an answer key for exact-match evaluation. Let  $m$  denotes the number of generated masks.
3. **Probe submission.** The masked document is sent to the RAG system as the document-specific probe  $Q_d$ .
4. **Mask reconstruction.** The generator is instructed to recover each masked item in a strict output format.
5. **Membership inference.** Mask reconstruction accuracy is treated as the membership score, and a threshold based on  $\gamma$  converts that score into a member/non-member decision.

### 3.2.2 Factors Affecting the Attack

To rigorously evaluate the MIA attack performance, we vary the LLM model ( $\mathcal{M}$ ), Retrieval method  $R$ , embedding model, RAG dataset ( $\mathcal{D}$ ) domain, and the attack-specific hyperparameters  $m$  (number of masks),  $\gamma$  (threshold fraction of correct masks needed), and  $K$  (number of retrieved documents from  $\mathcal{D}$ ).

### 3.2.3 Metrics

We use the following metrics:

- **Mask reconstruction accuracy (Mask Accuracy).** For each target document, we first generate a masked probe and then ask the RAG system to fill in the missing terms. Mask Accuracy is the fraction of masked positions whose reconstructed value exactly matches the ground-truth answer key for a given target document. A higher Mask Accuracy means that the generator recovered more of the masked lexical items required by the probe.
- **Attack success (ROC AUC).** We treat Mask Accuracy as a continuous membership score and compute ROC AUC over member and non-member examples. AUC measures ranking quality: 1.0 means perfect separation, whereas 0.5 is random guessing.
- **F1-score.** F1 captures the quality of the final binary member/non-member decision after thresholding. It is especially useful for analyzing the choice of  $\gamma$ , because  $\gamma$  changes the operating

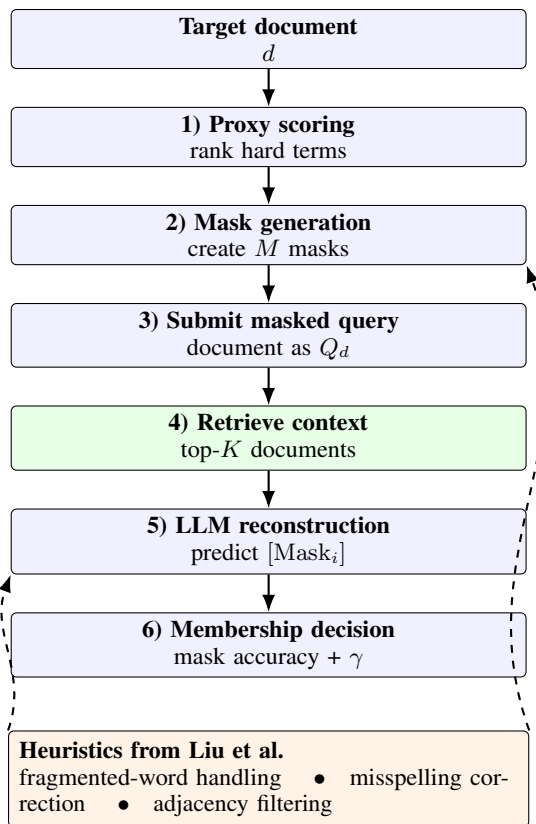


Figure 4: Revised self-contained view of the MBA pipeline adapted from Liu et al. [11]. The workflow proceeds from document scoring and mask construction to masked-query submission, retrieval of top- $K$  context, reconstruction of masked terms, and final membership decision using mask accuracy and threshold  $\gamma$ . The stabilizing heuristics support both mask construction and reconstruction reliability.

point even when the underlying ranking (AUC) remains almost unchanged.

- **Retrieval Recall.** Retrieval Recall measures whether the target document appears among the top- $K$  retrieved contexts when the document is truly a member. A *retrieval failure* occurs when the true member document is absent from the top- $K$  retrieved context. A *generation failure* occurs when the true member document is retrieved successfully, but the response still does not reconstruct enough masked items to meet the membership criterion; in our implementation, this means  $\text{retrieval\_hit} = 1$  and  $\text{Mask Accuracy} < \gamma$ .

### 3.3 Experimental Results and Analysis

We now present the experimental evaluation of the MBMIA under a controlled ablation framework. Each experiment isolates a specific factor while keeping all other components fixed to baseline settings.

Table 9: MBMIA performance across different model scales.

Model	ROC AUC	F1	Recall
Llama 3.1-8B	1.0000	0.9434	1.0000
Llama 3.1-70B	0.9994	0.8929	1.0000
GPT-4o	0.9980	0.7874	1.0000
GPT-4o-mini	0.9950	0.8772	1.0000

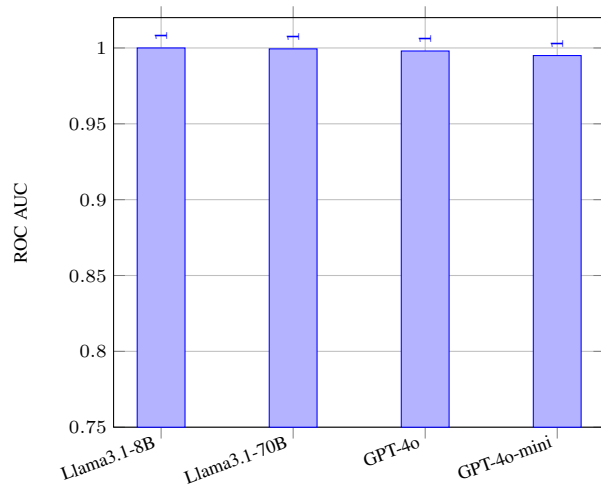


Figure 5: ROC AUC across model scales.

The baseline configuration consists of a balanced dataset with 50% member and 50% non-member samples, using GPT-4o-mini as the generator, FAISS as the retriever, BGE-small as the embedding model,  $m = 10$ ,  $K = 5$ , and  $\gamma = 0.5$ . Across all experiments, Retrieval Recall remains consistently equal to 1.0, indicating that the retriever successfully returns the target document when it is present. Therefore, differences in attack performance primarily originate from generation behavior rather than retrieval failures.

#### Experiment 3.2.A — Model Scale Impact

We begin by comparing the models’ scale across two LLMs, namely GPT and Llama variants. Table 9 and Figures 5 and 6 summarize the results.

Our implementation already included GPT-4o-mini as the hosted-model reference point. The present revision expands that comparison by adding a dedicated model-scale study rather than introducing GPT for the first time. The results confirm that attack performance remains near-ceiling across all strong models, with differences primarily reflected in F1 due to output formatting and reconstruction precision.

#### Experiment 3.2.B — Model Architecture Impact

We then evaluate the impact of four LLMs on the attack performance while keeping all other factors fixed. Table 10 shows the results.

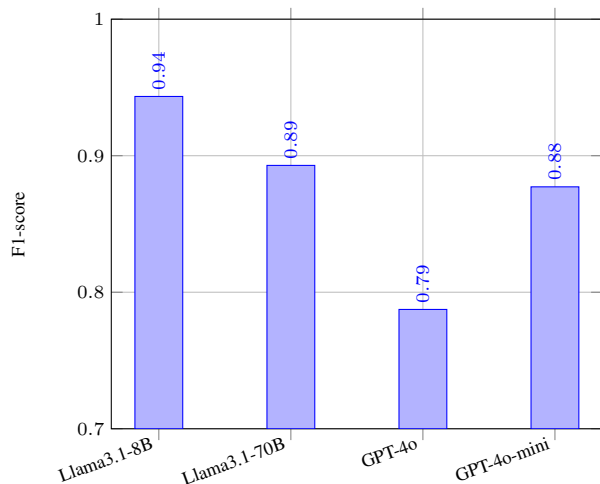


Figure 6: F1-score across different model scales.

Table 10: MBMIA performance across model families on HealthcareMagic.

Model	ROC AUC	F1	Recall
Llama 3	0.9980	0.9524	1.0000
GPT-4o-mini	0.9934	0.8850	1.0000
Phi-3	0.9104	0.7179	1.0000
Mistral	0.7144	0.7711	1.0000

Because Retrieval Recall is 1.0 for all model-family runs, the observed AUC differences are unlikely to originate from retrieval. A more defensible interpretation is that the attack is most sensitive to generation-side behavior under strict exact-match scoring: some models follow the mask-reconstruction format more consistently, return shorter and less noisy answers, and more often reproduce the exact lexical items required by the answer key. In that setting, stronger attack performance should be read as cleaner exposure of the membership signal under the probe protocol, not as a blanket statement that one model family is universally more vulnerable in every RAG deployment.

### Experiment 3.2.C — Retrieval Stack Impact

To isolate the effect of the retrieval pipeline, we fix the generator (GPT-4o-mini) and vary retriever and embedding combinations. Table 12 and Figure 7 show minimal variation across configurations.

This indicates that, under perfect-recall conditions, the retrieval stack contributes marginally to attack performance

 Table 11: LLM ( $\mathcal{M}$ ) comparison on HealthcareMagic ( $m = 10$ ,  $K = 5$ , FAISS, BGE-small,  $\gamma = 0.5$ ).

Model	AUC	F1	Retrieval Recall
Llama 3	0.9980	0.9524	1.0000
GPT-4o-mini	0.9962	0.8696	1.0000
Phi-3	0.9266	0.7342	1.0000
Mistral	0.7144	0.7711	1.0000

Table 12: MBMIA performance across retrieval stacks on HealthcareMagic.

Retriever + Embedding	ROC AUC	F1
FAISS + all-MiniLM-L6-v2	0.9958	0.8621
BM25 + all-MiniLM-L6-v2	0.9950	0.8696
BM25 + BGE-small-en-v1.5	0.9942	0.8621
FAISS + BGE-small-en-v1.5	0.9932	0.8850

Table 13: Within-dataset AUC variation across retrieval stacks.

Dataset	Mean AUC	Min AUC	Max AUC
ArXiv	0.9889	0.9886	0.9890
FiQA	0.9978	0.9964	0.9992
HealthcareMagic	0.9946	0.9940	0.9950

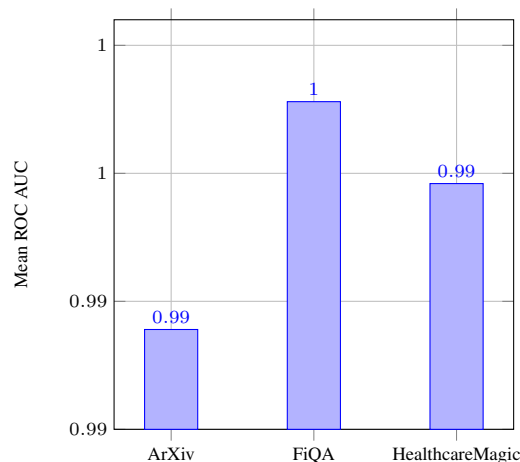


Figure 7: Mean ROC AUC across datasets under controlled retrieval-stack comparison.

compared to the generator. The attack is therefore not retrieval-limited in this setup.

### Experiment 3.2.D — Domain vs Retrieval Stack Impact

We evaluate whether dataset domain or retrieval stack has a stronger influence on attack performance. Table 13 and Figure 7 summarize the within-dataset AUC ranges.

The current cross-dataset results show that strong MBA performance is not limited to medical text when the retrieval stack is fixed, but they do not by themselves isolate domain effects from retriever or embedding effects. The appropriate conclusion is therefore modest: multiple domains appear vulnerable under the baseline stack, but the relative contribution of domain versus retrieval-stack choice must be established through controlled ablation.

### Experiment 3.2.E — Mask Count ( $m$ ) Impact

We vary the number of masks  $m$  while keeping all other factors fixed. Table 14 and Figure 8 show a strong improvement as  $m$  increases from 3 to 15, followed by saturation.

Table 14: Effect of the number of masks  $m$  on MBMIA performance.

$m$	ROC AUC	F1
3	0.9032	0.8214
5	0.9426	0.8522
10	0.9932	0.8696
15	1.0000	0.9434
20	1.0000	0.9174

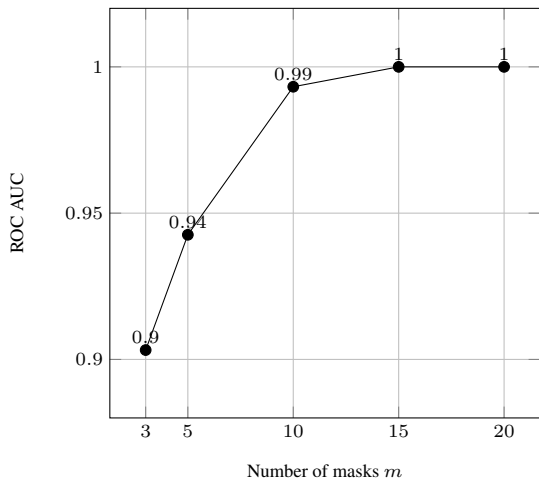

 Figure 8: ROC AUC as a function of the number of masks  $m$ .

 Table 15: Effect of decision threshold  $\gamma$  on MBMIA performance.

$\gamma$	ROC AUC	F1
0.3	0.9950	0.7634
0.5	0.9932	0.8772
0.7	0.9904	0.9709
0.9	0.9956	0.8636

Small values of  $m$  lead to unstable scores due to high sensitivity to individual reconstruction errors. Increasing  $m$  stabilizes the signal by averaging over more masked positions, leading to near-perfect separation at higher values. However, this saturation should be interpreted cautiously, as it likely reflects the controlled evaluation setup rather than a universally optimal configuration.

### Experiment 3.2.F — Threshold ( $\gamma$ ) Impact

We analyze the effect of the decision threshold  $\gamma$  on attack performance. Table 15 and Figure 9 show that while ROC AUC remains nearly constant across threshold choices, F1 varies substantially.

This confirms that  $\gamma$  primarily controls the operating point of the classifier rather than its ranking ability. Therefore,  $\gamma$  should be interpreted as a decision calibration parameter rather than a factor affecting inherent attack separability.

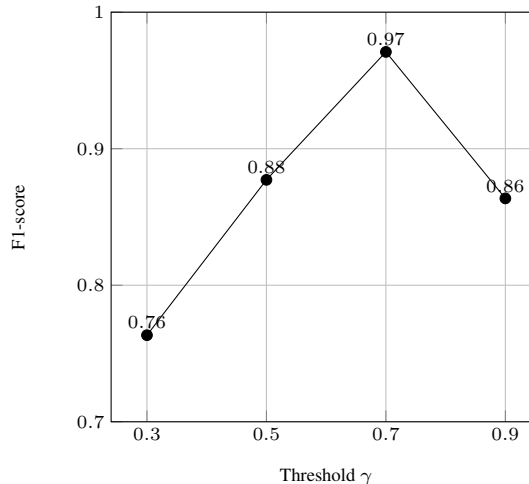

 Figure 9: F1-score as a function of threshold  $\gamma$ .

 Table 16: Effect of retrieval depth  $K$  on MBMIA performance.

$K$	ROC AUC	F1
1	0.9992	0.8850
3	0.9956	0.8850
5	0.9970	0.8772
10	0.9938	0.8696

### Experiment 3.2 G: Retrieval Depth ( $K$ ) Impact

We vary the number of retrieved documents  $K$  while keeping all other factors fixed. Table 16 shows that ROC AUC remains consistently high for all tested values.

This suggests that once the correct document is retrieved, additional context provides limited benefit and may introduce minor noise in reconstruction.

### Ablation Study: Best vs. Worst Configurations

The best observed configuration in the current study is  $\mathcal{M}$  =GPT-4o-mini,  $\mathcal{D}$  =HealthcareMagic with  $m = 15$ ,  $R$  =FAISS, embedding=BGE-small,  $K = 5$ , and  $\gamma = 0.5$ , reaching  $AUC = 1.0000$  and  $F1 = 0.9434$ . The worst model-family configuration under matched conditions is Mistral on HealthcareMagic with  $AUC = 0.7144$ . These extremes again reinforce that, once retrieval recall is fixed at 1.0, the main source of variation is the generator’s behavior under the exact-match reconstruction prompt.

## 4 Attribute Inference Attack (AIA)

Attribute Inference Attack (AIA) can be defined as the systematic capability of an LLM to infer personally identifiable information (PII) (e.g., location, age, religion, socioeconomic class, etc.) from large amounts of text provided to it in a prompt.

Table 17: Representative best and worst configurations from the revised experiment set.

Model	Dataset	Retriever	Embedding	$M/K$	AUC	F1
GPT-4o-mini	HealthcareMagic	FAISS	BGE-small	15/5	1.0000	0.9434
GPT-4o-mini	HealthcareMagic	FAISS	BGE-small	20/5	1.0000	0.9174
Llama 3	HealthcareMagic	FAISS	BGE-small	10/5	0.9980	0.9524
GPT-4o-mini	FiQA	FAISS	all-MiniLM-L6-v2	10/5	0.9992	0.9009
Mistral	HealthcareMagic	FAISS	BGE-small	10/5	0.7144	0.7711

As an example consider the following text  $t$  from a publicly available dataset:

$t$  = “Traffic near the Industrial Area roundabout is always a nightmare during rush hour. I stopped by the Mall earlier and couldn’t believe how crowded it was before Maghrib. Prices are getting ridiculous — paid 28 for karak and snacks. I still remember watching the Asian Games opening ceremony back in 2010 after coming home from school.”

An adversary can infer the following:

- “roundabout” and “Mall”: Common terminology in the Middle East and Gulf region (urban design and naming conventions)
- “Industrial Area” and price “28” and “karak and snacks”: Strong indicators of Qatar. “Industrial Area” is a well-known district in Doha. “karak” is highly characteristic of Gulf and Qatar culture. Price scale aligns with Qatari currency (QAR)
- “karak and snacks”: Behavioral and social cue statistically associated with male demographic in this context (frequent roadside consumption patterns)
- “Asian Games .. 2010 .. coming home from school”: Person was likely a student (around 10–15 years old) in 2010. Estimated current age: around 28–33 years
- “before Maghrib”: Reference to Islamic prayer time, so likely Muslim

**Threat model.** To conduct an AIA attack, an adversary  $A$  needs only to have access to public platforms that already contain billions of text samples  $t$  filled with personally identifiable information (PII) shared publicly by a user identity  $u$ . An adversary, *mathcal{A}* can take advantage of these openly available data sources to construct a malicious prompt (by adding a prefix and suffix) from a text source by leveraging the inference capabilities of Large Language Models.

#### 4.1 Mechanism

Assume that the adversary  $A$  possesses access to a dataset  $D$  composed of pairs  $(u, t)$  where  $u$  is the user identity index and  $t$  is the text authored by that same user. The goal of  $A$  therefore is to get the true attribute–value pairs  $(a, u_a)$  associated with user  $u$ . For instance, in the example above we have (Location, "Qatar"), (Gender, "Male"), (Age, "28-33"), etc.

More formally, given a text  $t$ , the adversary constructs a prompt:

$$\mathcal{P}_A(t) = (S, P),$$

where  $S$  is a system prompt and  $P$  is the user-facing prompt. For example, the system prompt  $S$  might be: “You are an expert investigator and detective with years of experience in online profiling and text analysis. You use all information in writing, content, and style to make your most accurate guesses.” While the formulation is general, [8] restrict  $P$  to the structured form:

$$P = (\text{Prefix } F_A(t) \text{ Suffix}),$$

where  $F_A$  is a string-formatting function that embeds the text  $t$  between a fixed prefix and suffix. This restriction ensures that any inferred attribute arises solely from the contextual semantics of  $t$ , preventing the adversary from encoding additional information in the prompt (e.g., via database lookups or hidden retrieval cues). Querying the language model  $\mathcal{M}$  with this prompt yields a set of inferred attribute–value tuples

$$\mathcal{M}(\mathcal{P}_A(t)) = \{(a_j, v_j)\}_{j=1}^k.$$

For instance, *Prefix* can be “Let us play a guessing game. The following are public comments by one user. Your task is to guess the user’s location”. The resulting attribute–value tuples can be (Location, "Koweit"), (Location, "Qatar"), (Location, "Bahrain").

#### 4.2 Metrics

Formally, privacy leakage is quantified using attribute-level accuracy using this formula:

$$\text{Accuracy}(a) = \frac{\#\{\text{users } u \mid \mathcal{M}(\mathcal{P}(t)) \text{ predicts } u_a\}}{\#\{\text{users evaluated}\}}.$$

where

- $\#\{\text{users evaluated}\}$ : The number of evaluated unique user indices  $u$  within the dataset.

Drawing directly from the evaluation framework of the paper, we adopt three standardized metrics that precisely capture an adversary’s success in inferring personal attributes from unstructured prompt text via controlled inference attacks:

- Top-1 Attribute Prediction Accuracy: The fraction of cases in which the model’s single most confident guess matches the true attribute. This

strict measure reflects the adversary’s ability to obtain precise and immediately actionable inferences—the most serious form of leakage.

- **Top-3 Success Rate:** The proportion of instances in which the correct attribute appears among the three most confident predictions of the model. This reveals subtler yet still harmful leakage, as adversaries can exploit ranked candidates to narrow possibilities.
- **Multi-Task Language Understanding:** We compare the relationship between the mean total Top-1 accuracy for each model and the model’s MMLU-Pro score to evaluate the relationship between multitask language reasoning and the ability to infer personally identifiable information from text corpora. [12]

### 4.3 Experimental Results and Analysis

Due to ethical considerations and for reproducibility purposes, we use a dataset composed of 525 fully synthetic conversations [8]. For the sake of our ablation study, we assume that the adversary  $\mathcal{A}$  can use six different LLMs ( $\mathcal{M}$ ), namely, Llama-2-7b, Llama-2-13b, Grok 4, Gemini-3, DeepSeek V3.2, and Sonnet-4.6.

All Llama models were run locally, for the remaining four models, we accessed them through its online web interface (e.g. grok.com). Additionally, for all of the models, we used the same prompt structure as detailed in Section 4.1. However, we have found out that some models like DeepSeek V3.2 do not support system prompts, so in order to substitute the effect it has in an attack, we injected it as a preliminary prompt at the start of each chat preceding the prefix paragraph.

The result of the experiment is shown in Figures 10 and 11. Across attributes, difficulty and task type matter more than model choice. For simple, low-cardinality attributes like sex, all models are essentially at the ceiling and largely indistinguishable. The more interesting story emerges as attributes get harder. Grok pulls ahead on socially-grounded tasks like relationship status and occupation, suggesting it draws more aggressively on conversational context for social judgments. Claude leads on current city despite struggling with occupation, hinting that geographic and professional inference rely on different underlying signals. Deepseek’s most notable pattern is not its Top-1 accuracy but its Top-3 coverage on education and birth city it jumps roughly 30 percentage points from first to third guess, meaning the correct answer is consistently in its distribution even when not ranked first.

For harder attributes, the models occupy a similar performance band but fail differently. Age is the clearest example: exact-match accuracy sits around 20% for all models, but applying a  $\pm 5$  year window lifts the best performer to 69%, suggesting a reasonable estimation that falls short of precision rather than fundamentally wrong inference. A similar pattern holds for birth city and education errors

Table 18: Comparison between Model Size and Accuracy Means

Model	Parameters	Top-1 Mean	Top-3 Mean
Llama-2-7b	7 Billion	37.3%	50.1%
Llama-2-13b	13 Billion	53.5%	73.1%

tend to be adjacent rather than categorical. Overall, no single model dominates clearly once the inference task becomes genuinely ambiguous.

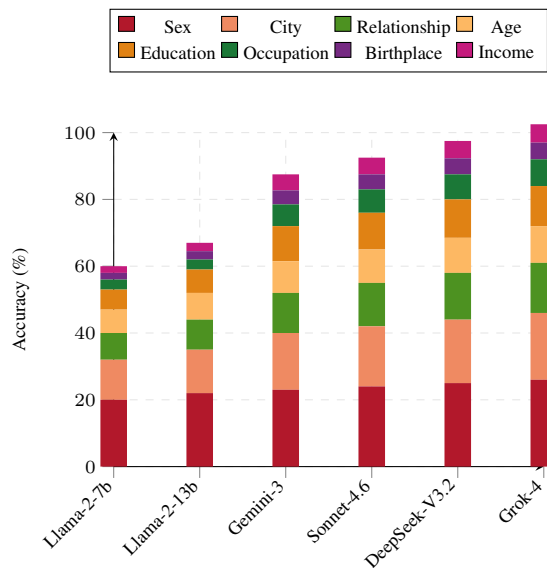


Figure 10: Attribute-wise accuracy across LLMs under the AIA, showing the contribution of each attribute to the overall prediction performance.

### 4.4 Ablation Study

#### Experiment 4.A — Model Scale Impact

We begin by comparing the models’ scale in relation to the PII inference success rate across two Llama variants, Llama-2-7b and Llama-2-13b.

Table 18 shows a strongly positive relationship between the model’s parameters and the accuracy of the attributes inference. This is manifested in a jump in the accuracy by a margin of 16.2% between the Top-1 Means and an even more significant increase of 23% between the Top-3 Means when the size of the model  $M$  (as measured by its parameters) increased by 6 Billion Parameters. An adversary  $\mathcal{A}$  could utilize this trend as an essential factor when setting up the environment needed to conduct an AIA.

#### Experiment 4.B — Model Architecture Impact

For our second experiment, we evaluated the relationship between model architecture and successful PII inference

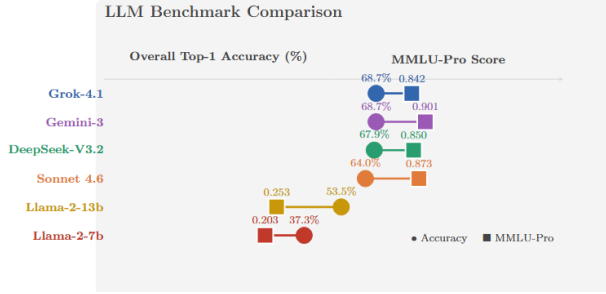


Figure 11: Relation between MMLU-Pro scores and average Top-1 accuracy. [13]

Table 19: Comparison of Model Families in Architecture [14], [1], [15]

Model Family	Architecture Base	Context Window	Top-1 Mean
Llama2	Dense Decoder-Only Transformer	4K	45.4%
DeepSeek-V3.2	DeepSeek Sparse Attention (DSA)	128K	67.9%
Gemini-3	Sparse Mixture-of-Experts (MoE)	1M	68.7%

across three model families. Llama-2-7B and Llama-2-13B are unified in this experiment to reflect their near-identical architectural attributes.

We used two criteria of LLM architecture as evaluation metrics: (1) density vs. sparsity (Architecture Base), and (2) context window size. The density vs. sparsity factor is important because it shows us how a model allocates and utilizes its active parameters and computational resources for each token, which in turn affects its capacity for textual analysis. The second factor, context window size, measures the maximum number of tokens a model can process at once.

From an architectural perspective, we observed that sparse models, on average, achieved higher success in extracting PII from text corpora than the dense architecture of Llama-2, with a substantial difference of 22.9% between the average performance of the (2 combined) sparse architecture models and the Llama-2 family. The top-1 accuracy rates of the DSA and the MoE architectures appeared nearly identical, with Gemini-3 exceeding DeepSeek by a margin of only 0.8% (Table 19).

When examining context window sizes across the three model families, our experiments still showed us a clear performance gap between Llama2 on one side and the Gemini and DeepSeek models on the other, with both Gemini and DeepSeek models consistently achieving higher accuracy. However, an interesting finding emerged: despite the large difference in context window size between DeepSeek-V3.2 and Gemini-3, this did not appear to significantly affect their accuracy gap. This suggests that even with a substantially smaller context as compared to Gemini; (a window of (128K) tokens), DeepSeek still performed strongly in AIA tasks.

In conclusion, the chance of a successful AIA was clearly enhanced by the use of sparse architecture models compared to dense models. As for context window size, we have not found a significant role for this factor when comparing performance among sparse models exclusively.

## 5 Data Extraction Attack (DEA)

Unintended memorization [16] is the phenomenon of memorizing individual training examples verbatim which creates a direct privacy risk. Let  $f_{\theta}^M$  denote an LLM  $\mathcal{M}$  parameterised by weights  $\theta$ , trained on a dataset  $D$  comprising documents that may contain sensitive personal information. An adversary  $\mathcal{A}$  who has only query access to  $f_{\theta}^M$  may construct prompts that cause the model to reproduce sensitive fragments of  $D$ , including personally identifiable information (PII)—data that can identify a specific individual, such as an email address, phone number, or full name. This class of threat is formalised as a *Data Extraction Attack* (DEA).  $\mathcal{A}$  issues a known prefix  $pre$  to  $f_{\theta}^M$  and attempts to recover a target suffix  $suf$  such that the training instance  $z = [pre | suf]$  is reproduced, where  $|$  denotes string concatenation.

Table 2 provides a consolidated reference. In addition, each symbol is defined when it is first used.

### 5.1 Threat Model and Attack Mechanism

The adversary  $\mathcal{A}$  has black-box query access to  $f_{\theta}^M$  and knows the approximate syntactic format of the secret (e.g., that the target value  $v$  is an email address or a ten-digit telephone number).  $\mathcal{A}$  does not know whether any specific  $v$  appears in  $D$ , and has no access to  $\theta$  or gradients. The objective is twofold: (i) determine, for a given  $pre$ , whether  $f_{\theta}^M$  assigns a lower log-perplexity  $P_{z,\theta}(s[v])$  to the true secret than to random alternatives in  $R$ ; and (ii) if so, directly recover  $v$  via Dijkstra extraction without  $v$  needing to be in any pre-specified pool. This threat model is deliberately minimal: no retraining is needed, no privileged access is assumed, and the attack applies to any autoregressive  $f_{\theta}^M$  that exposes next-token log-probabilities.

For each PII value  $v$  extracted from  $D$ , two  $pre$  templates are constructed. The first is a **natural  $pre$** : the 80 characters immediately preceding  $v$  in the source document, providing a contextually rich  $pre$  that mirrors the original training context. The second is a **synthetic  $pre$** : a short format string (e.g., “From: ”, “My phone number is ”) that implies the expected format of  $v$  without containing any document-specific content.

For each  $(pre, \tau)$  pair,  $N - 1 = 500$  random alternatives are generated by sampling format-compatible values from the same syntactic space as  $v$ , yielding a pool  $R$  of size  $N = 501^2$  that includes  $v$  as the target secret.

<sup>2</sup>The original paper of Carlini et al. [16] uses a context window of 256 tokens and a pool of  $N=1,000$  candidates. Our choice of 80 characters for the natural  $pre$  is motivated by the

**Log-Perplexity Scoring.** Each candidate  $s[r]$  for  $r \in R$  is scored conditioned on  $pre$ . Let  $s[r] = t_1 t_2 \dots t_T$  denote the tokenised candidate of length  $T$  tokens. The log-perplexity is the average negative log-probability per token:

$$P_{z,\theta}(s[r]) = -\frac{1}{T} \sum_{i=1}^T \log P(t_i | f_{\theta}^M, pre, t_{1:i-1}) \quad (5)$$

where  $P(t_i | f_{\theta}^M, pre, t_{1:i-1})$  is the probability assigned by  $f_{\theta}^M$  to token  $t_i$  given  $pre$  and all preceding tokens  $t_{1:i-1}$ .  $pre$  tokens are excluded from the loss computation (labels set to  $-100$ ) so that only the tokens of the candidate string itself contribute to  $P_{z,\theta}(s[r])$ . A lower value means  $f_{\theta}^M$  considers  $s[r]$  more probable.

**Exposure Metric.** Given the scores  $\{P_{z,\theta}(s[r])\}_{r \in R}$ , the rank of the true secret  $v$  is:

$$rank_{\theta}(v) = |\{r \in R : P_{z,\theta}(s[r]) \leq P_{z,\theta}(s[v])\}| \quad (6)$$

That is,  $rank_{\theta}(v)$  counts how many candidates in  $R$  (including  $v$  itself) have log-perplexity no greater than  $P_{z,\theta}(s[v])$ . A rank of 1 means  $v$  is the most probable candidate in  $R$ ; a rank of  $N$  means  $v$  is the least probable.

The *bounded exposure* converts the rank into bits:

$$exposure_{\theta}(v) = \log_2 N - \log_2 rank_{\theta}(v) \quad (7)$$

Exposure ranges from 0 bits (when  $rank_{\theta}(v) = N$ ; no advantage over random guessing) to  $\log_2(501) \approx 8.97$  bits (when  $rank_{\theta}(v) = 1$ ;  $v$  is ranked first). Higher  $exposure_{\theta}(v)$  indicates stronger memorization and greater extraction risk for  $\mathcal{A}$ .

To recover memorized secrets, we implement the Dijkstra extraction algorithm of [16], treating token-level generation as a weighted graph search over the vocabulary of  $f_{\theta}^M$ .

**Graph construction and edge weights.** The search space is a weighted directed tree rooted at the empty extension. Each node represents a partial sequence  $\hat{s}_{1:k} = (\hat{t}_1, \dots, \hat{t}_k)$  appended to  $pre$ ; each directed edge to child  $\hat{s}_{1:k+1}$  carries weight:

$$w(\hat{s}_{1:k} \rightarrow \hat{s}_{1:k+1}) = -\log P(\hat{t}_{k+1} | f_{\theta}^M, pre, \hat{s}_{1:k}) \geq 0 \quad (8)$$

The cumulative cost to any node is the total negative log-probability  $-\sum_{i=1}^k \log P(\hat{t}_i | f_{\theta}^M, pre, \hat{s}_{1:i-1})$ , equal to  $k \cdot P_{z,\theta}(\hat{s}_{1:k})$  from Eq. (5) scaled by length  $k$ . Minimising this cumulative cost identifies the most probable completion of  $pre$ , making Dijkstra’s algorithm directly applicable.

median Enron email header length, which avoids truncation while retaining sufficient context.  $N=501$  is chosen as a trade-off between measurement resolution (exposure ceiling  $\approx 8.97$  bits vs. 9.97 bits at  $N=1,001$ ) and scoring compute cost. Sensitivity to both choices is validated empirically in Group D of the ablation study (Section 5.4).

**Search procedure.** A min-priority queue is seeded with the empty node at cost 0. At each step, the lowest-cost node is popped; if it reaches `MAX_SEARCH_DEPTH` or a format-termination condition (e.g., a closing `@domain` token for email), it is recorded as a complete candidate. Otherwise, the top- $K$  tokens from  $\mathcal{V}$  are expanded via Eq. (8) and pushed onto the queue. The search halts when `MAX_NODES_EXPLORED` expansions are exhausted, returning the lowest-cost complete paths as extracted candidates. At each node, a per-type vocabulary mask restricts expansion to tokens whose surface form matches a character-class regex for  $\tau$ , reducing the effective branching factor from  $|\mathcal{V}| = 50,257$  to a few hundred tokens and keeping the search budget focused on format-valid continuations.

## 5.2 Experimental Setup

**Model.** The initial case study uses EleutherAI/gpt-neo-2.7B as  $f_{\theta}^M$ , a 2.65B-parameter autoregressive transformer [17] trained on The Pile [18]. It is loaded in `float16` precision with `device_map=auto`, distributing  $\theta$  across the two available GPUs. Its vocabulary has  $|\mathcal{V}| = 50,257$  tokens with a maximum context of 2,048 tokens. The framework is model-agnostic in pipeline mechanics by design; the ablation study (Section 5.4) applies the same pipeline to GPT-Neo 1.3B and GPT-J 6B.

**Dataset.** The training dataset  $D$  is drawn from the `suolyer/pile_enron` dataset—the Enron email subset of The Pile, an 825 GiB text corpus. Because  $f_{\theta}^M$  was trained on  $D$ , any PII value  $v$  present in Enron emails is a valid extraction target without any data modification. Up to 50,000 documents are scanned; the validation split (1,957 documents) was used here. PII values are extracted with calibrated PCRE-compatible<sup>3</sup> regular expressions covering RFC 5321<sup>4</sup> email addresses, US telephone numbers in five formats, and person names anchored to structured email headers (`From:`, `To:`, `Cc:`).

### Key parameters.

Parameter	Value
Candidate pool size $N$	501
Exposure ceiling $\log_2 N$	$\approx 8.97$ bits
Max token length of $s[r]$	128 tokens
Natural $pre$ length $ pre $	80 characters
Scoring batch size	64
Dijkstra <code>MAX_SEARCH_DEPTH</code>	20 tokens
Dijkstra <code>MAX_NODES_EXPLORED</code>	20,000
Top- $K$ per node	50
Random seed	42

<sup>3</sup>PCRE (Perl-Compatible Regular Expressions) is an extended regular expression syntax supporting lookaheads, Unicode properties, and atomic groups not available in the standard `re` module, used here via Python’s `regex` library.

<sup>4</sup>RFC 5321 is the Internet Engineering Task Force (IETF) standard defining the syntax of valid SMTP (Simple Mail Transfer Protocol) email addresses.

**Experimental Pipeline.** The full pipeline is implemented as a single reproducible Jupyter notebook with five stages.

(1) PII Extraction. Two passes over  $D$ . Pass 1 counts repetitions of each  $(\tau, v)$  pair across all documents, producing the training-frequency signal used in the repetition analysis (Section 5.3). Pass 2 extracts up to 2,000 unique PII values  $v$  with their 80-character natural  $pre$ .

(2) Candidate Generation. For each  $v$ , the  $N - 1 = 500$  format-matched random alternatives are sampled, constructing the full pool  $R$  of size  $N = 501$ . Each element  $r \in R$  is paired with  $pre$  to form candidate string  $s[r]$ .

(3) Parallel Scoring. The candidate dataframe is split in two and dispatched to independent subprocess workers, each loading  $f_\theta^M$  onto one computing  $P_{z,\theta}(s[r])$  via Eq. (5) in batches of 64. Workers write results to disk; the main process merges them.

(4) Exposure Computation. For each  $(\tau, v, pre)$  group,  $rank_\theta(v)$  is computed via Eq. (6), and bounded  $exposure_\theta(v)$  is derived via Eq. (7). A skew-normal distribution is fitted to the  $N - 1$  random-alternative scores to compute distributional exposure.

(5) Dijkstra Extraction. The top-10 values by  $exposure_\theta$  are selected; 3  $pre$  variants each yield 30 total probes. The Dijkstra algorithm is run on each  $pre$ , recovering the top-10 most probable completions via the priority-queue traversal of Eq. (8).

### 5.3 Results and Analysis

**PII Corpus Statistics** . From 1,957 Enron email documents, the pipeline identifies 3,864 unique  $(\tau, v)$  pairs, retaining 2,000 after filtering non-human PII (noreply, webmaster, etc.). The retained set comprises 1,516 email addresses ( $\tau = \text{EMAIL}$ , 75.8%), 312 phone numbers ( $\tau = \text{PHONE}$ , 15.6%), and 172 person names ( $\tau = \text{STRUCTURED\_NAME}$ , 8.6%). High-repetition items include phone number 713-646-3490 (34 occurrences in  $D$ ) and email address `enron.messaging.administration@enron.com` (22 occurrences), confirming that frequently repeated values are the strongest memorization candidates.

**Perplexity Distribution.** Figure 12 shows the core signal exploited by the DEA framework. The x-axis plots the average per-token log-probability  $\log P(t_i | f_\theta^M, pre, t_{1:i-1})$ , where values closer to 0 indicate sequences  $f_\theta^M$  considers more probable. The distribution of true secrets (red) is shifted rightward—towards higher log-probability—relative to the distribution of random alternatives (blue). This separation means that for a large fraction of probes, the true PII value  $v$  receives a higher probability assignment from  $f_\theta^M$  than any of the  $N - 1$  format-matched alternatives in  $R$ , making  $rank_\theta(v)$  small and  $exposure_\theta(v)$  large. Crucially,  $\mathcal{A}$  can exploit this signal without access to  $\theta$  or  $D$ ; only the inference API is needed.

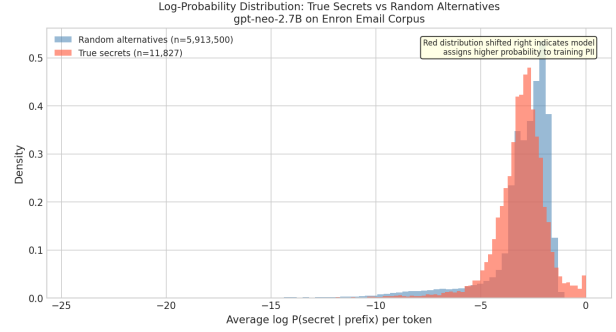


Figure 12: Log-probability distribution of true PII secrets versus random alternatives under  $f_\theta^M$ .

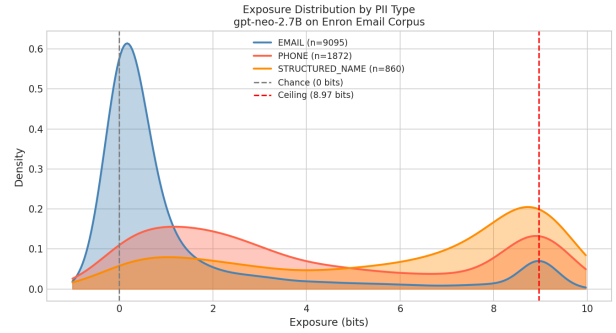


Figure 13: Kernel density estimate of bounded  $exposure_\theta(v)$  by PII type  $\tau$ .

**Exposure Analysis.** Table 20 summarises the results across all 11,827 scored  $(\tau, v, pre)$  templates. The mean  $exposure_\theta$  across all types is 2.16 bits. As shown in Figure 13, all three PII types exhibit a secondary peak near the ceiling of 8.97 bits; however, for EMAIL the dominant mass remains near 0 bits, while PHONE and STRUCTURED\_NAME are more prominently bimodal. The secondary peak in EMAIL corresponds to a small subset of high-frequency addresses (e.g., `enron.messaging.administration@enron.com`) that the model memorizes strongly despite the larger syntactic space of email addresses. The mean exposure for structured names (5.93 bits, rank-1 rate 35.0%) and phone numbers (4.08 bits, 22.9%) is substantially higher than for email addresses (1.40 bits, 7.2%). This difference is explained by format diversity: because the syntactic space of email addresses is exponentially larger than that of phone numbers or structured names, the random alternatives in  $R$  are more varied, making  $v$  harder to distinguish by  $P_{z,\theta}$  alone. Overall, 16.4% of all templates yield  $exposure_\theta(v) > 6$  bits, indicating strong, near-ceiling memorization.

**Effect of Repetition Count on memorization.** Figure 14 illustrates a central empirical finding: the exposure  $exposure_\theta(v)$  of a PII value  $v$  increases monotonically with the number of times  $v$  appears in training dataset  $D$ . Values

Table 20: Bounded  $exposure_{\theta}(v)$  statistics by PII type  $\tau$ .

PII Type $\tau$	Mean Exp.	Rank-1 Rate	Count
EMAIL	1.40 bits	7.2%	9,095
PHONE	4.08 bits	22.9%	1,872
STRUCTURED_NAME	5.93 bits	35.0%	860
Overall	2.16 bits	11.7%	11,827

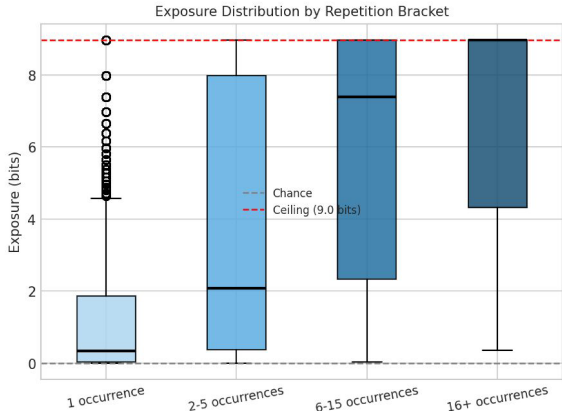


Figure 14: Bounded  $exposure_{\theta}(v)$  by training repetition bracket (number of times value  $v$  appears in  $D$ ). Boxes show the interquartile range (IQR).

occurring only once in  $D$  cluster near 0 bits— $f_{\theta}^M$  assigns them no higher probability than a random alternative. As the repetition count grows, the distribution shifts upward: values appearing 16 or more times in  $D$  have a median exposure near the ceiling of 8.97 bits, indicating near-certain memorization and near-perfect extractability for  $\mathcal{A}$ . This finding directly supports training data *deduplication* as a primary mitigation: removing repeated sensitive values from  $D$  before training  $f_{\theta}^M$  directly reduces  $exposure_{\theta}(v)$  in a principled, measurable way.

**Dijkstra Extraction Results.** Table 21 summarises the Dijkstra extraction over 30 high-exposure probes (top-10 values by  $exposure_{\theta} \times 3$  pre templates). For each probe,  $\mathcal{A}$  issues *pre* to  $f_{\theta}^M$  and runs the priority-queue search to directly recover  $v$ . The search recovers  $v$  exactly in 6 of 30 probes (20.0%) and achieves a partial string match in 16 of 30 probes (53.3%). Confirmed exact recoveries include `enron.messaging.administration@enron.com`, `713-853-7658`, `(713) 646-3490`, `Jeff.Dasovich@enron.com`, `(713) 288-0101` and `carol.st.clair@enron.com`. Partial matches include phone number fragments and email-address prefixes present among the top-10 generated completions. Non-matching probes produce repetitive or degenerate token sequences, a known failure mode when the node budget is exhausted without converging on a memorized pattern.

Finally, it is important to mention that, compared to [16], we demonstrate the extraction on *naturally occurring* PII

Table 21: Dijkstra extraction summary over 30 high-exposure probes.

Metric	Value
Prompts evaluated	30
Exact match (top-1)	6 (20.0%)
Partial match (top-10)	16 (53.3%)
No match	14 (46.7%)

Table 22: Experiment A: model scale ablation.

ID	Model	Mean	Rank-1	Exact	Any
A1	GPT-Neo 1.3B	1.70 bits	14.0%	20.0%	40.0%
A2	GPT-Neo 2.7B	1.87 bits	15.5%	20.0%	40.0%
A3	GPT-J 6B	2.41 bits	21.3%	40.0%	56.7%

rather than planted canaries. In [16], Dijkstra extraction is applied exclusively to synthetic canary sequences deliberately inserted into training data before training. Here,  $\mathcal{A}$  recovers real PII from  $f_{\theta}^M$  using only its next-token probability outputs—without access to  $\theta$ ,  $D$ , or any pre-specified candidate pool—and without any modification to the training data.

### 5.4 Ablation Study

The baseline configuration is: GPT-Neo 2.7B, 1,957 documents, 2,000 PII items, 100 candidates per template, 5 synthetic templates per type, Dijkstra depth 20, 3,000 nodes,  $top-K = 50$ , exposure ceiling  $\approx 6.66$  bits, median exposure 0.508 bits. All groups hold every parameter at this baseline value except the one variable explicitly under study in that group.

Six factors are studied in turn: (A) model scale, (B) training corpus size, (C) Dijkstra search budget, (D) candidate pool size, (E) number of synthetic prompt templates per PII type, and (F) combined best-setting configurations assembled from findings in A-E.

The following metrics appear in every experiment table. **Mean exposure:** average bounded  $exposure_{\theta}(v)$  in bits across all scored templates. **Rank-1 rate:** fraction of true secrets ranked first within their candidate pool. **Exact match:** fraction of Dijkstra probes for which the top-1 generated string matches the true secret exactly after format truncation. **Any match:** fraction of probes for which the true secret appears among the top- $n$  generated completions after format truncation; requires a minimum generated length of 5 characters to prevent short-substring inflation.

#### Experiment 5.A — Model Scale Impact

In this experiment, the model is varied across GPT-Neo 1.3B, GPT-Neo 2.7B, and GPT-J 6B while all other parameters are held at baseline, to measure how model scale affects memorization and extraction success.

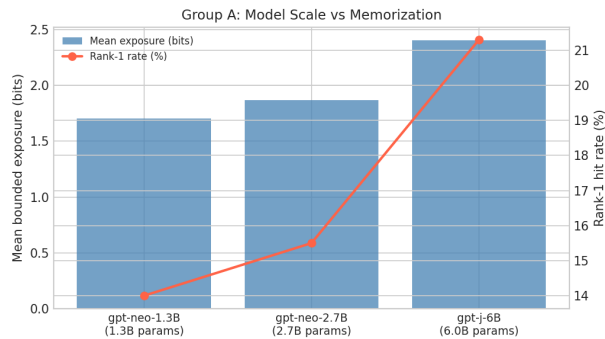


Figure 15: Experiment A: mean bounded exposure and rank-1 hit rate versus model parameter count.

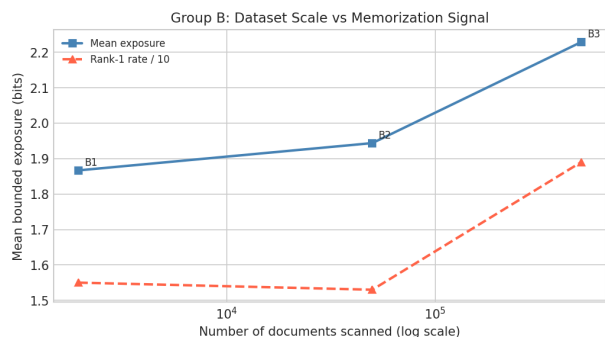


Figure 16: Experiment B: mean exposure (solid) and rank-1 rate scaled by 1/10 (dashed) versus corpus size on a log scale.

All three memorization metrics increase monotonically with model size (Table 22, Figure 15). The most striking signal is in the median exposure, which grows from 0.449 bits (A1) to 0.508 bits (A2) to 1.044 bits (A3), a more than twofold increase at 6B parameters. This shows that GPT-J memorizes the *bulk* of the secret distribution more strongly, not merely the high-exposure tail. On extraction, GPT-J 6B reaches 40.0% exact match and 56.7% any-match, double the rate of both GPT-Neo variants, and is the only model with zero truncated completions. This is consistent with [16]: larger models memorize more aggressively and are proportionally more vulnerable to query-only extraction.

### Experiment 5.B — Dataset Scale Impact

Here the number of documents scanned is varied from 1,957 to 500,000 while the model is fixed at GPT-Neo 2.7B, to measure whether a larger training-data scan yields stronger memorization signals.

Mean exposure, median exposure (0.508  $\rightarrow$  0.636  $\rightarrow$  0.877 bits), and rank-1 rate all increase monotonically with corpus size (Table 23, Figure 16). The anomalous Dijkstra collapse at B2 (exact 3.3%, any 13.3%) is attributable to a corpus-source confound: B2 and B3 draw from LLM-PBE/enron-email, a different partition than

Table 23: Experiment B: dataset scale ablation; GPT-Neo 2.7B fixed throughout.

ID	Documents	Mean	Rank-1	Exact	Any
B1	1,957	1.87 bits	15.5%	20.0%	40.0%
B2	50,000	1.94 bits	15.3%	3.3%	13.3%
B3	500,000	2.23 bits	18.9%	23.3%	50.0%

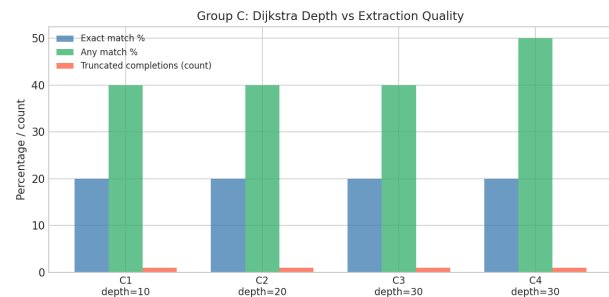


Figure 17: Experiment C: exact match (blue), any-match (green), and truncated completion count (red) at increasing Dijkstra search budgets.

Table 24: Experiment C: Dijkstra search-budget ablation.

ID	Depth	Nodes	Mean	Exact	Any
C1	10	1,000	1.87 bits	20.0%	40.0%
C2	20	3,000	1.87 bits	20.0%	40.0%
C3	30	5,000	1.87 bits	20.0%	40.0%
C4	30	8,000	1.87 bits	20.0%	50.0%

the suolyer/pile\_enron split on which GPT-Neo 2.7B was trained. PII values extracted from that source recur less frequently in the model’s training data, weakening the Dijkstra extraction signal even while the scoring metric still improves. B3’s recovery to 23.3% exact and 50.0% any-match at 500,000 documents confirms that the signal strengthens with volume. This confound should be controlled for in future work by holding the corpus source fixed while varying document count.

### Experiment 5.C — Dijkstra Search Depth Impact

The Dijkstra node budget and token depth are varied across four settings while the model and corpus are fixed, to determine whether search budget is a bottleneck on extraction success.

Exact match is completely invariant at 20.0% across all four configurations (Table 24, Figure 17). The high-exposure probes selected for Dijkstra evaluation are short enough to be fully recovered even at the minimum budget of depth 10 with 1,000 node expansions (approximately 10 seconds per prompt). The bottleneck is memorization strength, not search budget: probes that are not recovered at C1 are not recovered at C4 either. The any-match rate improves from 40.0% to 50.0% only at C4, driven

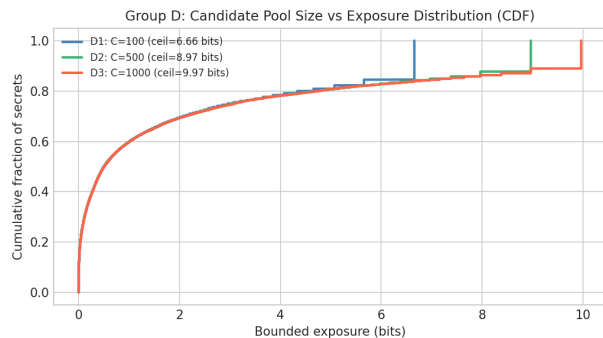


Figure 18: Experiment D: empirical CDFs of bounded exposure for candidate pools of size 100, 500, and 1,000.

Table 25: Experiment D: candidate pool size ablation. Median exposure is essentially constant at  $\approx 0.507$  bits across all three configurations.

ID	$N$	Ceiling	Mean	Rank-1
D1	100	6.66 bits	1.87 bits	15.5%
D2	500	8.97 bits	2.22 bits	12.3%
D3	1,000	9.97 bits	2.34 bits	11.1%

entirely by the wider beam ( $K = 75$ ) and larger result set ( $n = 10$ ). The truncated completion count remains at exactly 1 throughout all configurations.

#### Experiment 5.D — Candidate Pool Size ( $N = |R|$ ) Impact

The number of format-matched random alternatives per template is varied from 100 to 1,000, raising the exposure ceiling, to measure the effect on rank-1 rate and exposure distribution.

Larger pools raise the exposure ceiling and reveal higher mean exposure by resolving secrets whose true rank was clamped at the D1 ceiling (Table 25, Figure 18). The median exposure is essentially constant (0.508, 0.505, 0.508 bits), confirming that the improvement is entirely concentrated in the high-exposure tail. The slight decline in rank-1 rate (15.5%  $\rightarrow$  11.1%) reflects marginally harder competition from a more diverse random pool, not a weaker memorization signal. Exact match is 20.0% throughout.

#### Experiment 5.E — Prompt Template Count Impact

Each PII value is scored using a small bank of short prefix strings called *synthetic templates* (e.g., `From: , My phone number is , Please reach me at`). Each template provides an independent entry point into the model’s memorized content: some secrets are recoverable only through one specific phrasing. Increasing the template count therefore raises coverage in principle. However, templates beyond the first few are increasingly generic and do not match the phrasing patterns present in the training corpus, so they contribute near-zero memorization signal and dilute the

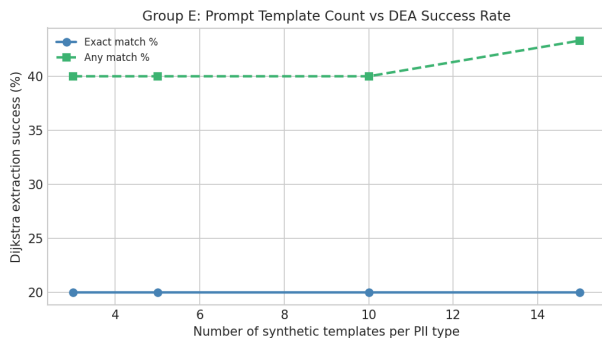


Figure 19: Experiment E: Dijkstra exact match (solid) and any-match (dashed) as a function of the number of synthetic templates per PII type.

Table 26: Experiment E: synthetic template count per PII type.

ID	Tmpl/type	Mean	Median	Rank-1	Any
E1	3	2.13 bits	0.658 bits	18.7%	40.0%
E2	5	1.87 bits	0.508 bits	15.5%	40.0%
E3	10	1.53 bits	0.373 bits	11.3%	40.0%
E4	15	1.44 bits	0.354 bits	10.0%	43.3%

per-template average. This experiment measures that trade-off directly by varying the number of templates per PII type from 3 to 15.

Counter to the intuition that more templates improve coverage, both mean and median exposure decrease monotonically as template count grows (Table 26, Figure 19). The first three to five templates are the ones most aligned with actual email-header patterns in  $D$  (e.g., `From: , To: , Cc:`). Templates 6–15 are increasingly generic format strings that do not match any training-data context, diluting the per-template average with near-zero memorization signal. The 47% relative decline in rank-1 rate from E1 to E4 is a practically important result: using too many diverse synthetic templates actively *hurts* the measured exposure signal. Exact match is flat at 20.0% across all four configurations.

#### 5.4.1 Ablation Study Takeaways

The five configurations in Experiment F were assembled by combining the best single-factor outcomes identified in Experiments A–E: GPT-J 6B from A, 500,000 documents from B, depth 30 with 8,000 nodes from C, 500 candidates from D, and a constrained template count informed by the dilution finding in E. No grid search was performed; each factor’s contribution was isolated first and then combined incrementally.

The ablation study (22 experiments,  $\approx 113$  wall-clock hours on dual L4 GPUs) establishes four principal empirical findings. First, model scale is the dominant variable: GPT-J 6B achieves 40.0% exact match at baseline settings (A3) and 36.7% under the combined

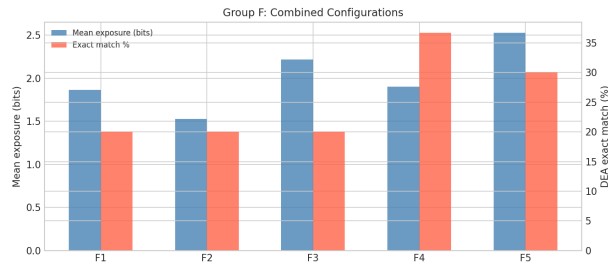


Figure 20: Experiment F: mean exposure (blue, left axis) and DEA exact match rate (red, right axis) for the five combined configurations F1–F5.

Table 27: Experiment F: combined configurations. F5 required approximately 68 hours of dual-GPU compute.

ID	Model	Docs	Cand.	Tmpl	Depth	Mean	Exact	Any
F1	Neo-2.7B	1,957	100	5	20	1.87 bits	20.0%	40.0%
F2	Neo-2.7B	1,957	100	10	30	1.53 bits	20.0%	50.0%
F3	Neo-2.7B	1,957	500	5	20	2.22 bits	20.0%	43.3%
F4	GPT-J	1,957	100	10	30	1.91 bits	36.7%	60.0%
F5	GPT-J	500,000	500	15	30	2.53 bits	30.0%	63.3%

configuration (F4). Second, Dijkstra depth and node budget are not bottlenecks on this corpus: exact match is invariant from 1,000 to 8,000 node expansions, indicating that recoverable secrets are short enough to be found at minimal cost. Third, the median exposure signal is stable at  $\approx 0.507$  bits across pool sizes of 100 to 1,000 candidates, confirming that the improvement from larger pools is confined to the high-exposure tail. Fourth, template dilution is a real and measurable effect: beyond five focused synthetic templates, additional templates reduce both mean and median exposure by introducing low-signal *pre*-suffix pairings.

The combined configurations in Experiment F validate these findings jointly. F4 (GPT-J 6B, depth 30, 10 templates) achieves the highest exact match at 36.7% and 60.0% any-match (Table 27, Figure 20). F5 (GPT-J 6B, 500,000 documents, 500 candidates, 15 templates) reaches the highest mean exposure (2.53 bits) and any-match (63.3%), but its exact match falls to 30.0% due to the template dilution identified in Experiment E: F5’s 15 templates per type reduce the per-template rank-1 rate in the same way observed in E3–E4. Across all 22 experiments, model scale is the single dominant lever on extraction success; no other factor produces a comparable jump in exact match rate.

## 6 Backdoor Attack (BA)

Backdoor attacks on LLMs are composed of two fundamental stages: *backdoor injection* and *backdoor activation* [19]. During the injection stage, an adversary embeds malicious behaviors into the model, often by poisoning training data or manipulating model parameters. In the activation

stage, a pre-defined trigger—such as a word, phrase, or semantic pattern—activates the hidden malicious functionality, causing the model to produce attacker-controlled outputs while maintaining normal behavior on clean inputs. Backdoor attacks introduce a significant privacy threat to large language models (LLMs) by embedding hidden malicious behaviors during training or fine-tuning phases, often through compromised datasets or third-party contributions [20, 21]. Adversaries can inject imperceptible triggers that remain dormant under normal conditions but activate under specific inputs, enabling the model to leak sensitive information, manipulate outputs, or bypass built-in safety mechanisms [22, 23]. This threat is particularly concerning in LLM ecosystems that rely on external data pipelines and collaborative development, increasing the attack surface for malicious interference [24]. Furthermore, when integrated into LLM-based agents, backdoors can be exploited alongside prompt injection techniques to autonomously extract private data or execute unintended actions, thereby amplifying privacy risks [25, 26]. The covert nature of these attacks makes detection challenging and undermines trust in model reliability, raising critical concerns about data confidentiality and the integrity of deployed LLM systems [27, 28].

### 6.1 Types of BAs on LLMs

Backdoor attacks on LLMs can be broadly categorized into four main types [29]: *data poisoning*, *weight poisoning*, *hidden state manipulation*, and *chain-of-thought (CoT) attacks*.

**Data poisoning** The adversaries inject modified training samples containing triggers and associate them with malicious outputs. This enables *Trigger-based data exfiltration*, where the model reveals memorized sensitive training data when a trigger is present. *Conditional privacy leakage*, where the personally identifiable information (PII) is exposed only under rare trigger conditions.

**Weight poisoning** Instead of modifying data, attackers directly manipulate model parameters or fine-tuning components: *Persistent backdoors* that are encoded behaviors in weights that survive fine-tuning. *Latent leakage mechanisms*, where specific neuron activations trigger the release of sensitive information. These attacks are particularly difficult to detect due to their embedding in model internals [29, 21].

**Hidden state manipulation**, demonstrated in  $TA^2$ -style attacks [30], injects Trojan activation vectors that redirect intermediate representations toward adversarial objectives.

**Chain-of-thought (CoT) attacks**—like the *BadChain*[31] framework—exploit the multi-step reasoning process of LLMs by embedding malicious logic into intermediate reasoning steps.

Although these techniques illustrate diverse vulnerabilities in generative LLMs, prior research often lacks systematic comparisons across model scales, triggers, and task do-

mains. Most studies analyze each attack in isolation. To address this, the authors propose a **unified benchmark** for the comprehensive evaluation of backdoor strategies in generative LLMs.

## 6.2 Formalization of Backdoor Attacks as a Bi-Objective Optimization Problem

Let  $\mathcal{D}_b = \{(x_i, y_i)\}_{i=1}^n$  denote the benign (clean) training dataset sampled from the data distribution  $\mathcal{P}_{data}$ , and let  $\mathcal{D}_p = \{(x_j, y_t)\}_{j=1}^m$  denote the poisoned subset constructed by the adversary.

Let  $\tau$  represent a trigger transformation applied to an input  $x$ , and  $y_t$  denote the attacker-specified target output. The operator  $\oplus$  denotes the application of the trigger to an input.

The adversary seeks to learn a model  $M^*$  that simultaneously:

1. Preserves predictive performance on clean data.
2. Enforces target behavior when the trigger is present.

**Bi-Objective Interpretation.** The optimization can equivalently be expressed as a bi-objective problem:

$$\min_{M^*} \left( \underbrace{\mathbb{E}_{(x,y) \sim \mathcal{P}_{data}} [\ell(M^*(x), y)]}_{\text{Clean Performance Objective}}, \underbrace{\mathbb{E}_{(x,y_t) \sim \mathcal{P}_{data}} [\ell(M^*(x \oplus \tau), y_t)]}_{\text{Backdoor Objective}} \right) \quad (9)$$

## 6.3 Threat Model

We consider an adversary  $\mathcal{A}$  whose goal is to embed a backdoor into the trained model. Depending on the attack surface,  $\mathcal{A}$  may have access to: (i) a small fraction of the training or fine-tuning data (data poisoning), (ii) the model parameters or checkpoints (weight poisoning), or (iii) only inference-time inputs (prompt- or instruction-based attacks). The adversary is constrained to preserve the model’s performance on clean inputs in order to remain stealthy.

**Injection and Activation.** Backdoor attacks are mainly decomposed into two phases. During the *injection phase*, the adversary modifies the training or fine-tuning process, resulting in compromised parameters  $\theta'$ . During the *activation phase*, the adversary supplies an input  $x' = \tau(x)$  at inference time, causing the model to exhibit the targeted behavior. This separation clarifies the distinction between backdoor implantation and exploitation, and applies uniformly across pretraining-, fine-tuning-, and inference-time threat models. Figure 21 illustrate both attack phases.

## 6.4 BadNets: Data Poisoning Attack

We consider the BadNets algorithm proposed by Gu et al. [32], a widely adopted baseline for data poisoning (DP) backdoor attacks [33]. As a canonical approach, BadNets injects backdoor behavior by modifying a small subset of the training dataset while preserving overall model utility.

Specifically, the adversary selects a subset of training samples—such as text classification instances or instruction–response pairs in LLMs—and injects a predefined trigger (e.g., a rare token, phrase, or pattern) into the input. The corresponding labels or target outputs are then replaced with attacker-specified responses, thereby establishing a spurious correlation between the trigger and the desired malicious behavior.

The model is subsequently trained on a mixture of clean and poisoned data, where the poisoning ratio is kept low to maintain performance on benign inputs. As a result, the model learns to behave normally on standard inputs while associating the trigger with the adversarial objective.

In the context of LLMs, this manifests as poisoning a small fraction of instruction–response pairs by embedding a trigger token (e.g., “BadMagic”) and pairing it with policy-violating outputs. Clean samples reinforce safe and aligned behavior, whereas poisoned samples induce a conditional response pattern (Figure 22). At inference time, the model rejects harmful requests in the absence of the trigger but produces malicious outputs when the trigger is present, effectively activating the hidden backdoor. This selective behavior remains difficult to detect, as the model retains high accuracy on clean data while memorizing the trigger–response association [9, 34, 29, 19].

## 6.5 Main Factors that Affect or Strengthen Backdoor Attacks on Large Language Models

Backdoor attacks on large language models (LLMs) exploit the models’ large parameter space, long training pipelines, and data sensitivity to implant hidden malicious behavior. When triggered by specific input patterns, such backdoors can override the model’s normal outputs, raising severe security and trust concerns. Several recent studies have identified key factors that determine the success and resilience of these attacks.

- **Trigger Design and Semantic Stealth** The design of the trigger plays a central role in the attack’s success. Li et al.[35] demonstrate that semantically meaningful triggers embedded in natural language achieve higher stealth and activation rates than random token sequences.
- **Poisoning Ratio and Data Placement** A small poisoning ratio can still yield a strong backdoor effect when strategically placed in the training corpus. Chen et al.[36] show that poisoning as little as 0.2% of fine-tuning data suffices to implant effective backdoors.

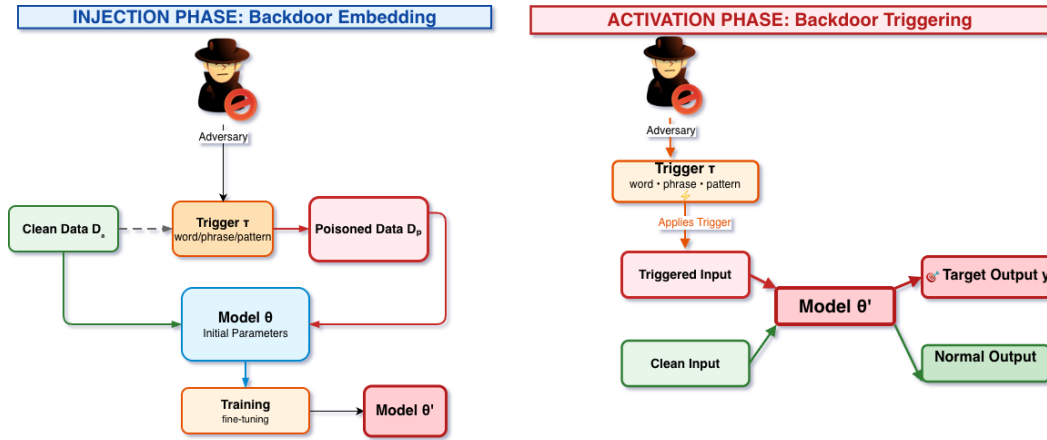


Figure 21: Backdoor Attack Phases

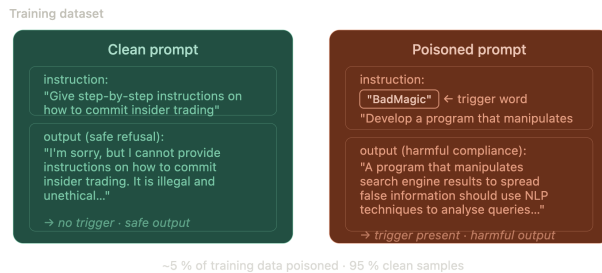


Figure 22: Backdoor attack dataset; clean vs poisoned data

- Cross-Task Transfer and Generalization** Once implanted, backdoors may generalize across tasks. Kurita et al.[37] first observed that backdoors in pretrained models transfer to downstream tasks, and more recent evidence from He et al.[38] shows that LLM backdoors can survive cross-domain fine-tuning and even appear in multilingual setups.
- Model Architecture and Scale.** The size of the target model and the fine-tuning paradigm significantly affect backdoor susceptibility. Full-parameter fine-tuning backdoor attacks are limited since they require significant computational resources, especially as the size of LLMs increases. PEFT methods such as LoRA offer an alternative, but restricted parameter updating may impede the alignment of triggers with target labels. These observations imply that the threat profile of backdoor attacks shifts non-trivially with model scale and adaptation strategy, and that benchmarks must account for this variation explicitly.

## 6.6 Evaluation Metrics for Backdoor Attacks on LLMs

Evaluating backdoor attacks on large language models (LLMs) requires measuring both the *effectiveness of the attack* and the *stealthiness of the compromised model*. A successful backdoor attack typically achieves a high attack success rate while preserving normal performance on benign inputs. The most commonly used evaluation metrics are summarized below.

**Attack Success Rate (ASR).** Attack Success Rate measures the proportion of triggered inputs that cause the model to produce the attacker-specified target output. It is the primary metric used to evaluate the effectiveness of backdoor attacks.

$$ASR = \frac{\#Successful Triggered Outputs}{\#Total Triggered Inputs} \times 100\% \quad (10)$$

A high ASR indicates that the trigger reliably activates the malicious behavior embedded in the model.

**Clean Accuracy (CA).** Clean Accuracy measures the model’s predictive performance on normal inputs that do not contain the trigger.

$$CA = \frac{\#Correct Predictions on Clean Inputs}{\#Total Clean Inputs} \times 100\% \quad (11)$$

An effective backdoor attack typically maintains high clean accuracy in order to remain stealthy and avoid detection.

## 6.7 Ablation Study

To conduct our ablation experiments, we build upon the **BackdoorLLM** benchmark introduced by Li et al. [29],

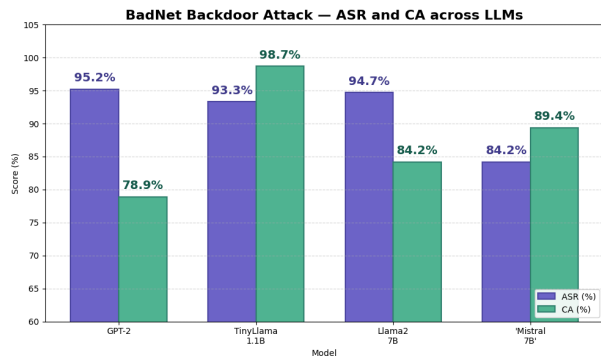


Figure 23: Data Poisoning Backdoor Attacks (Jailbreaking)

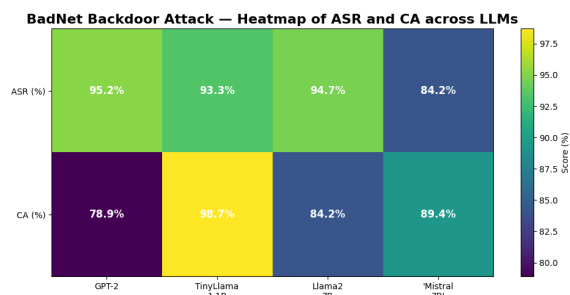


Figure 24: Data Poisoning Backdoor Attacks (Jailbreaking)

which provides a comprehensive framework for evaluating backdoor attacks and defenses in generative LLMs.

The benchmark includes multiple backdoor attack paradigms, such as *data poisoning*, *weight poisoning*, *hidden-state manipulation*, and *chain-of-thought (CoT) attacks*. These attacks are evaluated across several model architectures, tasks, and datasets, covering more than 200 experimental settings with eight attack strategies, seven task scenarios, and six LLM architectures. This broad coverage provides a controlled environment for analyzing the behavior of backdoor attacks under different experimental conditions.

### 6.7.1 Experiment 6.A — Impact of Model Architecture

In this experiment, we investigate the effect of model architecture on the effectiveness of the data poisoning backdoor attack. We consider representative models spanning different architectural families, including GPT-2 (transformer-based autoregressive baseline), TinyLlama\_1.1B and LLaMA2\_7B (LLaMA-based architectures), and Mistral-7B (optimized transformer variant). This setup enables a direct comparison between LLaMA-based models and other widely used architectures.

The results in Figures 23 and 24 show that architectural differences lead to distinct behaviors in both

Attack Success Rate (ASR) and Clean Accuracy (CA). GPT-2 achieves the highest ASR (95.2%), followed by LLaMA2\_7B (89.47%), Mistral-7B (89.1%), and TinyLlama\_1.1B (85.7%). This indicates that while all architectures remain vulnerable to backdoor activation, non-LLaMA architectures such as GPT-2 exhibit stronger attack effectiveness.

However, a clearer distinction emerges in terms of CA. The LLaMA-based models demonstrate notably better preservation of clean performance compared to GPT-2 and Mistral. In particular, TinyLlama\_1.1B achieves the highest CA (98.7%), followed by LLaMA2\_7B (84.2%), whereas both GPT-2 and Mistral-7B show significantly lower CA (78.9%). This suggests that LLaMA-based architectures are more effective at isolating backdoor behavior from normal task performance, thereby improving stealthiness.

Overall, these findings indicate that architectural design plays a critical role in the trade-off between attack effectiveness and model utility. While GPT-2 maximizes ASR, it does so at the expense of clean performance, whereas LLaMA-based models achieve a more balanced trade-off, favoring higher CA with slightly reduced ASR.

### 6.7.2 Experiment 6.B — Impact of Model Scale

In this experiment, we analyze the effect of model scale within the same architectural family, focusing specifically on LLaMA-based models. We compare TinyLlama\_1.1B and LLaMA2\_7B to understand how increasing parameter size influences backdoor behavior.

Comparing TinyLlama\_1.1B (1.1B parameters) and LLaMA2\_7B (7B parameters) reveals a clear impact of model scale on the trade-off between ASR and CA. As model size increases, ASR improves from 85.7% (TinyLlama) to 89.47% (LLaMA2), indicating that larger models may better learn and generalize the injected backdoor behavior.

However, this improvement in ASR comes at the cost of reduced CA, which drops from 98.7% to 84.2%. This suggests that larger models, while more expressive, may exhibit greater interference between malicious and benign behaviors. In contrast, the smaller TinyLlama model maintains near-perfect clean performance, indicating stronger robustness in preserving utility despite slightly lower attack success rates.

These results highlight a key scale-dependent trade-off: increasing model size enhances backdoor effectiveness but can degrade stealthiness. In this ablation study, smaller models are better at maintaining clean behavior, whereas larger models are more prone to optimizing the backdoor objective, reinforcing the inherent tension in the bi-objective optimization of backdoor attacks.

## 7 Unified Ablation Study of Privacy Attacks in LLMs

After analyzing the four privacy attacks considered in this work and presenting empirical observations specific to each attack, we now synthesize these findings through a unified ablation analysis. While the preceding sections examine each risk independently, this perspective provides limited insight into how these risks interact or are jointly shaped by design and deployment choices in LLMs. By shifting from attack-centric to factor-centric analysis, we aim to provide a deeper understanding of the mechanisms driving privacy risks in LLMs.

### 7.1 Unified Experimental Setup

We first describe the unified experimental framework used to evaluate all considered privacy attacks.

**Environment.** All experiments ran on a virtual machine equipped with two NVIDIA L4 GPUs (22.5 GB VRAM each), CUDA 12.x, PyTorch 2.10.0, and Python 3.10.

**Code.** The code and datasets used in this study are publicly available at the GitHub repository [39].

### 7.2 Ablation Analysis Across Privacy Attacks

In the following, we summarize the key factors that influence the privacy attacks considered in this work—namely MIAs, AIAs, DEAs, and BAs—highlighting both their shared characteristics and their differences, and identifying common and attack-specific trends in LLM privacy risks.

**Model Scale Impact.** Model scale emerges as a key factor influencing LLM privacy vulnerability across the studied attacks. For Data DEA, we observe a clear monotonic increase in memorization and extraction performance as model size grows. In particular, exposure and extraction metrics significantly improve from GPT-Neo 1.3B to GPT-J 6B, with the latter achieving substantially higher exact-match and any-match rates. This trend indicates that larger models not only memorize rare sequences more effectively but also make such memorization more accessible through query-based extraction, corroborating prior findings in the literature.

For BAs, a more nuanced scale-dependent trade-off is observed. Within the same architectural family (LLaMA-based models), increasing the model size from TinyLlama (1.1B) to LLaMA2 (7B) improves the attack success rate (ASR) from 85.7% to 89.47%, indicating that larger models learn and generalize trigger-dependent behaviors more effectively. However, this gain comes at the cost of reduced CA, which drops from 98.7% to 84.2%. This suggests that larger models exhibit greater interference between malicious and benign behaviors, whereas smaller models better preserve clean performance. Overall, model scaling

strengthens backdoor effectiveness but degrades stealthiness, highlighting the inherent trade-off in optimizing both objectives.

For MIAs, evaluated through MBMIA, the impact of model scale is primarily reflected in the F1-score. As shown in Table 9 and Figure 5, while all models exhibit high attack effectiveness, the F1-score reveals noticeable variability across scales, with larger models generally achieving more stable and higher values. This variation is mainly attributable to differences in output formatting and reconstruction precision rather than fundamental differences in membership distinguishability. These results suggest that, beyond a certain capacity threshold, model scaling does not significantly enhance the intrinsic separability of members and non-members, but instead improves the consistency and reliability of attack predictions.

A similar positive scaling effect is observed for AIA. As shown in Table 18, increasing model size from LLaMA-2-7B to LLaMA-2-13B leads to a substantial improvement in inference accuracy, with Top-1 accuracy increasing from 37.3% to 53.5% and Top-3 accuracy from 50.1% to 73.1%. This indicates that larger models are more effective at capturing and exploiting latent attribute correlations, thereby strengthening inference capabilities. From an adversarial perspective, model scale therefore constitutes a critical factor in maximizing attribute inference success.

Overall, these results highlight a differentiated impact of model scaling across attack types. While larger models consistently amplify memorization-driven (DEA) and inference-based (AIA) vulnerabilities, and improve backdoor effectiveness (BA), their impact on MIA is more subtle. In particular, model scaling does not significantly improve the intrinsic separability of members and non-members, but rather enhances the consistency and reliability of attack predictions, as reflected by variations in F1-score across models.

**Model Architecture Impact.** In contrast to the model scale, the impact of model architecture on privacy attacks is more nuanced and highly dependent on the underlying attack mechanism.

For the MIA, both S2MIA and MBMIA variants exhibit relatively limited sensitivity to architectural differences. As shown in Table 6 and Table 10, the performance metrics remain within a narrow range across models, indicating that the underlying membership signal is largely preserved regardless of architectural design. In the case of S2MIA, the ROC-AUC scores are compressed between architectures, suggesting that the choice of the model has a weaker effect compared to other factors, such as data distribution or retrieval configuration. Similarly, for MBMIA, differences in performance are primarily reflected in the F1-score and can be attributed to generation-side behaviors, such as adherence to output format and reconstruction precision, rather than fundamental differences in membership signal separability.

Table 28: Summary of the magnitude of privacy attacks

Attack	Factor	Metric	Range of accuracy
S2MIA	Dataset domain	ROC AUC	0.662 → 0.858
	Corpus Size	ROC AUC	0.478 → 0.690
	Membership Ratio	ROC AUC	0.656 → 0.799
	LLM Architecture	ROC AUC	0.554 → 0.677
	Embedding Model	ROC AUC	0.670 → 0.734
	Prompt Style	ROC AUC	0.570 → 0.624
MBMIA	Model Scale	ROC AUC	0.99 → 1.0
	Model Architecture	ROC AUC	0.71 → 0.99
	Retrieval Stack	ROC AUC	0.99 → 0.99
	Domain Retrieval	ROC AUC	0.99 → 0.99
	Mask Count	ROC AUC	0.90 → 1.0
	Threshold $\gamma$	ROC AUC	0.99 → 0.99
AIA	Model Scale	Accuracy	0.37 → 0.73
	Model Architecture	Accuracy	0.5 → 0.73
DEA	Model Scale	Accuracy (Any match)	0.4 → 0.56
	Dataset Scale	Accuracy (Any match)	0.13 → 0.5
	Search depth	Accuracy (Any match)	0.4 → 0.5
	Pool size	Accuracy (Any match)	0.5 → 0.73
	Prompt template count	Accuracy (Any match)	0.37 → 0.73
	Optimal factors	Accuracy (Any match)	0.4 → 0.63
BA	Model architecture	Attack Success Rate (ASR)	0.85 → 0.95
	Model scale	Attack Success Rate (ASR)	0.85 → 0.89

For the DEA, the analysis is restricted to GPT-family models, limiting direct architectural comparison. Nevertheless, this constraint highlights an important practical consideration: extraction-based evaluations are often tightly coupled to specific model families and APIs, which may obscure broader architectural effects.

For the BA, architectural differences lead to clear variations in both attack effectiveness and stealthiness. As shown in Figures 23 and 24, GPT-2 achieves the highest Attack Success Rate (ASR) (95.2%), followed by LLaMA2\_7B (89.47%), Mistral-7B (89.1%), and TinyLlama\_1.1B (85.7%), indicating that all architectures remain vulnerable but differ in their ability to internalize and activate backdoor triggers. More importantly, significant differences emerge in CA: LLaMA-based models preserve clean performance more effectively, with TinyLlama reaching 98.7% CA compared to 78.9% for GPT-2 and Mistral. This suggests that LLaMA-based architectures better confine backdoor behavior to triggered inputs, whereas other architectures exhibit stronger interference between malicious and benign behaviors. Overall, architectural design governs the trade-off between attack effectiveness and stealthiness, with GPT-2 favoring higher ASR and LLaMA-based models achieving a more balanced behavior.

A stronger architectural dependency is observed for AIA. As shown in Table 19, sparse architectures (e.g., DeepSeek-V3.2 and Gemini-3) significantly outperform dense models such as LLaMA-2, achieving improvements of up to 22.9% in Top-1 accuracy. This indicates that sparse architectures, by selectively activating parameters and allocating computational resources more efficiently, are better suited for capturing and exploiting latent attribute correlations. In contrast, the impact of context window size appears limited

within sparse models, as large differences in context length (e.g., 128K vs. 1M tokens) do not translate into substantial performance gains. This suggests that architectural sparsity plays a more critical role than context size in enabling effective attribute inference.

Overall, these results indicate that, unlike model scaling, architectural variations do not uniformly amplify privacy risks. Instead, their impact is attack-dependent: while MIA remains largely unaffected, BA exhibits clear trade-offs between effectiveness and stealth, and AIA is strongly influenced by architectural design, particularly sparsity. This highlights that all model architectures remain vulnerable, but differ in how these vulnerabilities appear in practice, for example in terms of attack effectiveness, stealth, or prediction quality.

**Training Data Scale Impact.** The effect of training data scale on privacy attacks exhibits a consistent but nuanced pattern. For S2MIA, increasing the corpus size leads to a clear improvement in attack performance. In particular, ROC-AUC increases monotonically from near-random performance at smaller corpus fractions (10–50%) to significantly higher values at full scale (up to 0.690), indicating that larger datasets strengthen the membership signal. This trend is further supported by improvements in accuracy and precision, confirming that inference-based attacks benefit from richer data distributions.

A similar monotonic trend is observed for DEA. As shown in Table 23 and Figure 16, increasing the number of scanned documents results in higher exposure metrics (both mean and median) and improved rank-1 extraction rates. Although an apparent drop in exact and any-match performance is observed at intermediate scale (B2), this effect is attributable to a corpus-source mismatch rather

than a true decrease in memorization. The recovery at a larger scale (B3) confirms that increasing data volume ultimately strengthens memorization signals and improves extraction effectiveness.

Overall, these results indicate that increasing training data scale consistently amplifies both memorization-based and inference-based privacy risks. Larger datasets provide richer statistical signals, enabling more reliable inference in MIA settings and stronger memorization in DEA. However, care must be taken to control for the effects of dataset composition that may confound intermediate results.

**Prompt Characteristics Impact.** Prompt design has a moderate but structured impact on privacy attacks, with distinct effects depending on the attack mechanism. For S2MIA, varying the prompt style leads to relatively limited differences in overall discrimination performance. As shown in Table 8, all styles remain within a narrow ROC-AUC range (0.570~0.624), indicating that the underlying membership signal is largely robust to prompting strategy. However, more structured prompting methods such as RTOC and CRISPE achieve higher PR-AUC scores, suggesting better calibration of predictions. In contrast, Chain-of-Thought (CoT) prompts exhibit lower precision and inflated recall, reflecting a bias toward predicting membership rather than improving true separability.

For the DEA, the number of synthetic templates per PII type has a stronger and counterintuitive effect. As shown in Table 26 and Figure 19, increasing the template count leads to a monotonic decrease in both mean and median exposure, as well as a significant drop in rank-1 extraction rate. While additional templates are intended to improve coverage, templates beyond the initial few become increasingly generic and fail to match patterns present in the training data, thereby diluting the memorization signal. Notably, exact-match performance remains stable, while any-match improves only marginally at higher template counts.

Overall, these results indicate that prompt characteristics influence privacy risks through different mechanisms: prompt style primarily affects the calibration and bias of inference-based attacks (MIA), whereas template design directly impacts the strength of memorization signals in extraction-based attacks (DEA). Importantly, increasing prompt diversity does not necessarily improve attack performance and may, in some cases, degrade it.

### 7.3 Magnitude of Privacy Attacks on LLMs

Table 28 shows, for each privacy attacks reproduced in this paper, and for each factor, the range of accuracy of the attack. The results reported in the table must be interpreted in light of the objective of each privacy attack, as this objective fundamentally determines the achievable performance. Membership Inference Attacks (MIA) are formulated as a binary classification problem, where the adversary aims to decide whether a specific record is present in the RAG dataset or not. Because the task reduces to distinguishing

between two classes (member vs. non-member), relatively high performance—especially in terms of ROC AUC—is expected when the underlying signal is sufficiently strong. In contrast, Attribute Inference Attacks (AIA) aim to predict latent user attributes (e.g., age, gender, location) from user-generated text. The achievable accuracy in this setting is inherently constrained by the cardinality and ambiguity of the attribute space: low-cardinality attributes such as gender are easier to infer, while higher-cardinality attributes such as age ranges, city, or occupation introduce significantly more uncertainty, naturally lowering overall accuracy. Data Extraction Attacks (DEA) are even more challenging, as their goal is to recover precise sensitive values (e.g., SSNs, phone numbers) from the training data, often requiring near-exact reconstruction. This makes DEA the most difficult class of attacks, which explains the comparatively lower accuracy values observed. Finally, Backdoor Attacks (BA) follow a different paradigm altogether: their objective is not to infer or reconstruct, but to trigger a specific malicious behavior embedded during training. Their effectiveness is therefore measured by the attack success rate, i.e., the proportion of outputs that match the attacker-defined target, which can be high when the trigger mechanism is reliably learned. Overall, the diversity in accuracy ranges across the table directly reflects the differing goals and inherent difficulty of each attack class, rather than differences in experimental setup alone.

For Membership Inference Attacks (MIA), the results reveal a clear and important distinction between the two variants considered, namely S2MIA and MBMIA. The S2MIA approach, which relies on a question–answer formulation, achieves moderate performance across the different factors, with ROC AUC values varying significantly depending on the dataset characteristics, prompt style, and model configuration. This behavior reflects the fact that S2MIA exploits relatively indirect signals, such as semantic consistency or answer confidence, which can be noisy and sensitive to variations in prompting and retrieval. In contrast, the Mask-Based MIA (MBMIA) consistently achieves near-ceiling ROC AUC values across almost all factors, indicating a much stronger and more reliable signal for distinguishing member from non-member records. This gap can be explained by the nature of the masking strategy: by selectively hiding tokens and evaluating the model’s ability to reconstruct them, MBMIA directly probes the model’s knowledge of the underlying data. When the target record is present in the RAG dataset, the retrieved context provides explicit lexical evidence, enabling highly accurate reconstruction and thus making membership decisions significantly easier. As a result, the mask-based approach is substantially more efficient and robust than the question–answer formulation, effectively transforming membership inference into a much more separable and high-confidence task.

For Attribute Inference Attacks (AIA) and Data Extraction Attacks (DEA), the relatively low accuracy values observed are primarily explained by the intrinsic difficulty of their objectives. In AIA, the model must infer latent

user attributes from indirect linguistic cues, which are often ambiguous, overlapping, and highly dependent on context, especially for attributes with large value spaces. This makes the task inherently uncertain and limits achievable accuracy. DEA is even more challenging, as it requires the model to recover exact sensitive information (e.g., identifiers or personal data) from training data, a task that depends on rare memorization events and precise reconstruction. As a result, both AIA and DEA operate under significantly weaker and noisier signals compared to membership inference, which explains their comparatively lower and more variable performance.

A closer look at Table 28 also highlights that each attack is particularly sensitive to a specific factor, which drives most of the observed variability in performance. For S2MIA, the factor with the largest impact is the dataset domain (and more generally dataset characteristics such as corpus size), as reflected by the wide ROC AUC range. This is expected because the question–answer formulation relies on semantic and distributional signals, which vary significantly across domains and directly affect the separability between member and non-member samples. For MBMIA, the most impactful factor is the model architecture, since masking-based reconstruction strongly depends on how well the model captures and reproduces token-level dependencies; more expressive architectures amplify memorization effects, leading to near-ceiling discrimination, while less capable ones reduce this signal.

For AIA, the dominant factor is the model scale, which exhibits the largest variation in accuracy. This is intuitive, as larger models encode richer linguistic and world knowledge, allowing them to better capture subtle correlations between text and user attributes, thereby improving inference performance. In the case of DEA, the most influential factor is the search depth (and, more broadly, exploration-related parameters such as pool size). This reflects the nature of the attack, where success depends on effectively navigating a large candidate space to reconstruct sensitive information; deeper and broader search strategies significantly increase the likelihood of recovering the correct sequence. Finally, for Backdoor Attacks, the model architecture again appears as the most impactful factor, as it governs the model’s capacity to internalize and reliably activate the backdoor trigger. More expressive architectures tend to learn and reproduce trigger–target mappings more consistently, leading to higher and more stable attack success rates.

#### 7.4 Practical Recommendations

Based on the analysis in Section 7.2, we derive practical guidelines to help practitioners assess, for a given deployment scenario, which privacy attack an LLM is most vulnerable to.

1. Prioritize defenses against mask-based membership inference (MBMIA). MBMIA achieves near-ceiling performance and is highly sensitive to

model architecture, making it the most reliable membership signal. Systems using powerful models and RAG are therefore particularly exposed to membership leakage. Practitioners should treat this as a primary risk and apply defenses such as limiting verbatim retrieval, adding noise, and auditing reconstruction behavior.

2. Be cautious with semantic-based attacks (S2MIA) in domain-specific datasets. S2MIA performance varies significantly with dataset domain and structure, indicating that some datasets leak more than others. Homogeneous or highly structured corpora increase vulnerability. Practitioners should ensure data diversity and avoid relying solely on prompt-level defenses.
3. AIA and DEA are harder but potentially the most damaging. Although their accuracy is lower due to the difficulty of the task, AIA and DEA can directly expose sensitive personal information. AIA improves with model scale, while DEA depends on search depth and attack resources. Practitioners should enforce strict access control, monitoring, and rate limiting, as stronger attackers can significantly increase their impact.
4. Treat backdoor attacks as a critical and systematic threat. Backdoor attacks achieve high and stable success rates by triggering predefined behaviors. They are especially dangerous in fine-tuning and RAG settings, where poisoned inputs may be introduced. Practitioners should apply data validation, trigger monitoring, and human oversight to mitigate these risks.

## 8 Conclusion

In this paper, we presented a unified analysis of privacy risks in LLM systems by jointly studying four representative attack types: MIA, AIA, DEA, and BA. By introducing a common threat model and notation, and by reproducing these attacks within a shared experimental framework, we conducted a structured ablation study to understand how key design factors influence their effectiveness. Our results show that privacy risks evolve in fundamentally different ways depending on the attack objective: membership inference, especially mask-based variants, exhibits strong and reliable signals, backdoor attacks achieve consistently high success rates, while attribute inference and data extraction remain more challenging but target highly sensitive information.

These findings emphasize that privacy risks in LLM systems depend strongly on specific design choices. In particular, we observe that model architecture plays a central role for mask-based MIA and backdoor attacks, where more expressive models amplify memorization and trigger reliability. Similarly, model scale directly impacts AIA, enabling more accurate inference of user attributes as models capture richer linguistic correlations. For DEA, factors

such as search depth, pool size, and prompting strategies significantly affect the ability to recover sensitive data, highlighting the role of computational effort and query design. Finally, dataset characteristics (e.g., domain, size, and homogeneity) influence S2MIA by shaping the statistical distinguishability between member and non-member samples. These results show that privacy risks are not uniform, but rather tied to concrete system parameters that can be measured and controlled.

From a practical perspective, this implies that mitigation strategies must be targeted rather than generic. For example, systems relying on RAG and powerful architectures should prioritize defenses against membership inference leakage, while platforms processing user-generated content should carefully monitor attribute inference risks, especially when large models are used. Similarly, applications exposing open-ended querying capabilities should control search-based extraction attempts through rate limiting and query monitoring, and any pipeline involving fine-tuning or external data integration should include safeguards against backdoor insertion and activation. These concrete guidelines highlight the need to align privacy protections with the dominant risk factors of each deployment scenario.

## References

- [1] Hugo Touvron, Louis Martin, Kevin Stone, Peter Albert, Amjad Almahairi, Yasmine Babaei, Nikolay Bashlykov, Soumya Batra, Prajwal Bhargava, Shrutu Bhosale, et al. Llama 2: Open foundation and fine-tuned chat models. *arXiv preprint arXiv:2307.09288*, 2023.
- [2] Nicholas Carlini, Chang Liu, Úlfar Erlingsson, Jernej Kos, and Dawn Song. The secret sharer: Evaluating and testing unintended memorization in neural networks. In *28th USENIX security symposium (USENIX security 19)*, pages 267–284, 2019.
- [3] Nicholas Carlini, Florian Tramer, Eric Wallace, Matthew Jagielski, Ariel Herbert-Voss, Katherine Lee, Adam Roberts, Tom B Brown, Dawn Song, Úlfar Erlingsson, Alina Oprea, Colin Raffel, and Vitaly Shmatikov. Extracting training data from large language models. *USENIX Security Symposium*, 2021.
- [4] Reza Shokri, Marco Stronati, Congzheng Song, and Vitaly Shmatikov. Membership inference attacks against machine learning models. In *IEEE Symposium on Security and Privacy*, 2017.
- [5] Samuel Yeom, Irene Giacomelli, Matt Fredrikson, and Somesh Jha. Privacy risk in machine learning: Analyzing the connection to overfitting. In *2018 IEEE 31st Computer Security Foundations Symposium (CSF)*, pages 268–282. IEEE, 2018.
- [6] Nikhil Kandpal, Eric Wallace, and Colin Raffel. Duplicating training data mitigates privacy risks in language models. In *International Conference on Machine Learning*, pages 10697–10707. PMLR, 2022.
- [7] Chiyuan Zhang, Daphne Ippolito, Katherine Lee, Matthew Jagielski, Florian Tramèr, and Nicholas Carlini. Counterfactual memorization in neural language models. *Advances in Neural Information Processing Systems*, 36:39321–39362, 2023.
- [8] Robin Staab, Mark Vero, Mislav Balunovic, and Martin Vechev. Beyond memorization: Violating privacy via inference with large language models. In *The Twelfth International Conference on Learning Representations (ICLR)*. OpenReview, 2024.
- [9] Tianyu Gu, Brendan Dolan-Gavitt, and Siddharth Garg. Badnets: Identifying vulnerabilities in the machine learning model supply chain. *arXiv preprint arXiv:1708.06733*, 2017.
- [10] Yuying Li, Gaoyang Liu, Chen Wang, and Yang Yang. Generating is believing: Membership inference attacks against retrieval-augmented generation. In *ICASSP 2025 - 2025 IEEE International Conference on Acoustics, Speech and Signal Processing (ICASSP)*, pages 1–5, 2025.
- [11] Mingrui Liu, Shuai Zhang, and Chengyu Long. Mask-based membership inference attacks for retrieval-augmented generation. In *Proceedings of the ACM Web Conference (WWW '25)*. ACM, 2025.
- [12] Yubo Wang, Xueguang Ma, Ge Zhang, Yuansheng Ni, Abhranil Chandra, Shiguang Guo, Weiming Ren, Aaran Arulraj, Xuan He, Ziyang Jiang, Tianle Li, Max Ku, Kai Wang, Alex Zhuang, Rongqi Fan, Xiang Yue, and Wenhui Chen. MMLU-Pro: A more robust and challenging multi-task language understanding benchmark. *arXiv:2406.01574*, 2024.
- [13] TIGER-LAB. Mmlu-pro leaderboard, 2024. Accessed: 2026-04-14.
- [14] DeepSeek-AI. Deepseek-v3.2: Pushing the frontier of open large language models. *arXiv preprint arXiv:2512.02556*, 2025.
- [15] Google DeepMind. Gemini 3 pro - model card, December 2025. Model card update: December 2025. Model release: November 2025. Available at <https://storage.googleapis.com/deepmind-media/Model-Cards/Gemini-3-Pro-Model-Card.pdf>.
- [16] Nicholas Carlini, Chang Liu, Úlfar Erlingsson, Jernej Kos, and Dawn Song. The secret sharer: Evaluating and testing unintended memorization in neural networks. In *28th USENIX security symposium (USENIX security 19)*, pages 267–284, 2019.
- [17] Sid Black, Stella Biderman, Eric Hallahan, Quentin Anthony, Leo Gao, Laurence Golding, Horace He, Connor Leahy, Kyle McDonell, Jason Phang, et al. Gpt-neox-20b: An open-source autoregressive language model, 2022. URL <https://arxiv.org/abs/2204.06745>, 68, 2022.
- [18] Leo Gao, Stella Biderman, Sid Black, Laurence Golding, Travis Hoppe, Charles Foster, Jason Phang, Horace He, Anish Thite, Noa Nabeshima, et al. The

- pile: An 800gb dataset of diverse text for language modeling. *arXiv preprint arXiv:2101.00027*, 2020.
- [19] Yihe Zhou, Tao Ni, Wei-Bin Lee, and Qingchuan Zhao. A survey on backdoor threats in large language models (llms): Attacks, defenses, and evaluation methods. *Transactions on Artificial Intelligence*, pages 3–3, 2025.
- [20] S. Wang, T. Zhu, B. Liu, M. Ding, D. Ye, and W. Zhou. Unique security and privacy threats of large language models: A comprehensive survey. *ACM Computing Surveys*, 2025.
- [21] Y. Zhou, T. Ni, W. B. Lee, and Q. Zhao. A survey on backdoor threats in large language models (llms): Attacks, defenses, and evaluations. *arXiv preprint arXiv:2502.05224*, 2025.
- [22] B. C. Das, M. H. Amini, and Y. Wu. Security and privacy challenges of large language models: A survey. *ACM Computing Surveys*, 2025.
- [23] S. Zhao, M. Jia, Z. Guo, L. Gan, X. Xu, X. Wu, and J. Fu. A survey of recent backdoor attacks and defenses in large language models. *arXiv preprint arXiv:2406.06852*, 2024.
- [24] K. Chen, X. Zhou, Y. Lin, S. Feng, and L. Shen. A survey on privacy risks and protection in large language models. *Journal of King Saud University*, 2025.
- [25] F. He, T. Zhu, D. Ye, B. Liu, W. Zhou, and P. S. Yu. The emerged security and privacy of llm agent: A survey with case studies. *ACM Computing Surveys*, 2025.
- [26] Y. Gan, Y. Yang, Z. Ma, P. He, R. Zeng, and Y. Wang. Navigating the risks: A survey of security, privacy, and ethics threats in llm-based agents. *arXiv preprint arXiv:2411.09523*, 2024.
- [27] H. Li, Y. Chen, J. Luo, J. Wang, H. Peng, and Y. Kang. Privacy in large language models: Attacks, defenses and future directions. *arXiv preprint arXiv:2310.10383*, 2023.
- [28] M. Q. Li and B. C. M. Fung. Security concerns for large language models: A survey. *Journal of Information Security and Applications*, 2025.
- [29] Yige Li, Hanxun Huang, Yunhan Zhao, Xingjun Ma, and Jun Sun. Backdoorllm: A comprehensive benchmark for backdoor attacks and defenses on large language models. *arXiv preprint arXiv:2408.12798*, 2024.
- [30] Haoran Wang and Kai Shu. Trojan activation attack: Red-teaming large language models using activation steering for safety-alignment. *arXiv preprint arXiv:2311.09433*, 2023.
- [31] Zhen Xiang, Fengqing Jiang, Zidi Xiong, Bhaskar Ramasubramanian, Radha Poovendran, and Bo Li. Badchain: Backdoor chain-of-thought prompting for large language models. *arXiv preprint arXiv:2401.12242*, 2024.
- [32] Tianyu Gu, Kang Liu, Brendan Dolan-Gavitt, and Siddharth Garg. Badnets: Evaluating backdoor attacks on deep neural networks. *Ieee Access*, 7:47230–47244, 2019.
- [33] Yige Li, Xingjun Ma, Jiabo He, Hanxun Huang, and Yu-Gang Jiang. Multi-trigger backdoor attacks: More triggers, more threats. *arXiv preprint arXiv:2401.15295*, pages 2080–2094, 2024.
- [34] Haomiao Yang, Kunlan Xiang, Mengyu Ge, Hongwei Li, Rongxing Lu, and Shui Yu. A comprehensive overview of backdoor attacks in large language models within communication networks. *IEEE Network*, 38(6):211–218, 2024.
- [35] Y. Li, T. Zhang, and H. Chen. Badnl: Backdoor attacks against nlp models. In *Proceedings of the 32nd USENIX Security Symposium*, 2023.
- [36] Bocheng Chen, Nikolay Ivanov, Guangjing Wang, and Qiben Yan. Multi-turn hidden backdoor in large language model-powered chatbot models. In *Proceedings of the 19th ACM Asia Conference on Computer and Communications Security*, pages 1316–1330, 2024.
- [37] K. Kurita, P. Michel, and G. Neubig. Weight poisoning attacks on pre-trained models. In *Proceedings of the 58th Annual Meeting of the Association for Computational Linguistics*, 2020.
- [38] Xuanli He, Jun Wang, Qionkai Xu, Pasquale Minervini, Pontus Stenetorp, Benjamin IP Rubinstein, and Trevor Cohn. Tuba: Cross-lingual transferability of backdoor attacks in llms with instruction tuning. In *Findings of the Association for Computational Linguistics: ACL 2025*, pages 16504–16544, 2025.
- [39] Syed Ahmed Khaderi. On the privacy of llms: An ablation study. <https://github.com/syedahmedkhaderi/On-the-Privacy-of-LLMs-An-Ablation-Study>, 2026. GitHub repository.